Effects of hot electrons on the stability of a closed field line plasma

by
Natalia S. Krasheninnikova
B.S. Physics, Applied Mathematics, Pure Mathematics, and Computer Science,
University of Massachusetts, Boston (1998)

Submitted to the Nuclear Science and Engineering Department
in partial fulfillment of the requirements for the degree of
Doctor of Philosophy in Applied Plasma Physics
at the

MASSACHUSETTS INSTITUTE OF TECHNOLOGY
January 2006 (February 2007)

Author.....
Nuclear Engineering Department
January 20, 2006

Certified by.....
Peter J. Catto
Senior Research Scientist, Theory Head and Assistant Director of the PSFC
Thesis Supervisor

Certified by.....
Jeffrey P. Freidberg
Professor of Nuclear Science and Engineering Department
Thesis Supervisor

Certified by.....
Jay Kesner
Senior Research Scientist, Physics Research Group Leader, LDX
Thesis Reader

Accepted by.....
Professor Jeffrey A. Coderre
Chairman, Department Committee on Graduate Students

Effects of hot electrons on the stability of a closed field line plasma

by

Natalia S. Krasheninnikova

B.S. Physics, Applied Mathematics, Pure Mathematics, and Computer Science,

University of Massachusetts, Boston (1998)

Submitted to the Nuclear Science and Engineering Department on January 20, 2006,
in partial fulfillment of the requirements for the degree of
Doctor of Philosophy in Applied Plasma Physics

Abstract

Motivated by the electron cyclotron heating being employed on dipole experiments, the effects of a hot species on stability in closed magnetic field line geometry are investigated. The interchange stability of a plasma consisting of a fluid background with a population of kinetic hot electrons is considered. The species diamagnetic drift and magnetic drift frequencies are assumed to be of the same order, and the wave frequency is assumed to be much larger than the background drift frequencies.

To illustrate the key physics issues and obtain an simpler understanding of instability mechanisms, we first examine the effects of hot electrons in cylindrical Z-pinch geometry. This linear approximation to a dipole preserves the essential feature of closed magnetic field lines. The absence of variations along the equilibrium magnetic field allows us to analytically derive an arbitrary total pressure dispersion relation, investigate a large variety of regimes, and explain the physical phenomena at work. Our analysis finds that two different types of resonant hot electron effects can modify the simple Magnetohydrodynamic (MHD) interchange stability condition. When the azimuthal magnetic field increases with radius, there is a critical pitch angle above which the magnetic drift of the hot electrons reverses. The interaction of the wave with the hot electrons with pitch angles near this critical value always results in instability. When the magnetic field decreases with radius, magnetic drift reversal is not possible and only low speed hot electrons interact with the wave. Destabilization by this weaker resonance effect can be avoided by carefully controlling the hot electron density and temperature profiles.

Based on the insights obtained by considering a Z-pinch, we then expand our calculation to a dipole magnetic field confined plasma by retaining geometrical effects such as the poloidal variations of electric and magnetic fields. These variations cause quasi-neutrality and the radial component of Ampere's law to become a set of coupled integro-differential equations which without approximations can only be solved numerically. To obtain a semi-analytic solution we consider an interchange approximation that allows us to obtain an arbitrary beta dispersion

relation that recovers the correct Z-pinch limit. In the dipole case, our analysis again shows that a weak drift resonance with slowly moving hot electrons can result in destabilization, which can be controlled by the hot electron density and temperature profiles. The specific example of a point dipole equilibrium is considered in some detail to explicitly demonstrate these results. In contrast with the Z-pinch, a strong hot electron destabilization due to magnetic drift reversal is found not to occur in a point dipole.

Thesis Supervisor: Peter J. Catto
Title: Senior Research Scientist, Theory Head and Assistant Director of the PSFC

Thesis Supervisor: Jeffrey P. Freidberg
Title: Professor of Nuclear Science and Engineering Department

Dedicated to the memory of D. J. S.

ACKNOWLEDGMENTS

I wanted to express my most sincere gratitude to my research supervisor Dr. Peter Catto. Over the past few years, he has not only guided my research through what sometimes seemed to be an impassable debris, but has also became a father figure to me. His PATIENCE (in capital letters), kindness and support are unsurpassable. He was always quick with a word of encouragement when I stumbled, and a "swift, heavy hand" when I strayed from the right path. I was extremely fortunate to be given an opportunity to learn plasma physics from him, as this experience allowed me to gain a great deal of knowledge about theoretical approach in general and kinetic theory in particular. I am also very grateful to him for being taught what a proper paper should look like. Though I cannot make a promise of putting all "the's" and "a's" in the right place, or not writing a page-long sentences, I believe that his teachings will stay with me for the rest of my life. From the bottom of my heart, Thank You, Peter!

I am extremely grateful to Dr. Jay Kesner's (MIT) interest and numerous discussions about the applications and physical interpretations of our results to the LDX experiment, particularly his helpful comments that led to the generalization of our results to $\beta_h >> \beta_b$, as well as hot electron interchange mode. His way of understanding of our analysis was very unique, and helped breach the gap between the world of theory and experiment for me. I will also treasure our informal political discussions about Russia, and America. Thank You, Jay!

I also wanted to express my sincere gratitude to Prof. Dieter Sigmar, who encouraged and helped me to attend MIT and to whom this work is dedicated, though unfortunately too late.

I am very grateful to Prof. Jeffrey Friedberg for his encouragement and support during the earlier stages of this work.

I would like to thank Dr. Andrei Simakov (LANL) for numerous discussions as well as his eager help with computational part of this work.

I am also grateful to Dr. Darrien Garnier and Dr. Mike Mauel for their interest in our work and helpful suggestions.

I wanted to thank Jim Hastie (Culham) for discussions in the initial phase of this work and Prof. Kim Molvig and Dr. Abhay Ram (MIT) for stimulating Landau resonance discussions.

Finally, I want to thank my family: my husband Shawn and daughter Ekaterina Vinyard, my parents and brother, and my parents-in-law for their loving support. I also want to thank my friends and colleagues Vincent Tang, Jerry Hughes, Alex Kouznetzov, Kirill Zhurovich and Paul Foster for their helpful discussions and making it possible to stay in the office without windows for so long.

This research was supported by the U.S. Department of Energy grant No. DE-FG02-91ER-54109 at the Plasma Science and Fusion Center of the Massachusetts Institute of Technology

Contents

List of Figures

Chapter 1

Introduction

The motivation behind this work is the recent interest in the Levitated Dipole Experiment (LDX) operating at MIT. It has been built by Columbia University and MIT to investigate the physics of plasmas confined by a dipolar magnetic field and to explore the possibility of achieving high plasma pressure comparable to the magnetic pressure[1,2]. To confine plasma this device uses a dipolar magnetic field, created by a superconducting coil that is capable of producing up to 4 Tesla of magnetic field with the average of a few tenths of a Tesla. Presently, the coil is being supported, but it is expected to be levitated in the current year, which will reduce the losses to the supports and improve confinement[18]. LDX is shown schematically in Fig. 1.1. It has a chamber radius of about 2.5 m, a levitated coil outer diameter of 1.2 m, and it contains approximately 30 m^3 of plasma.

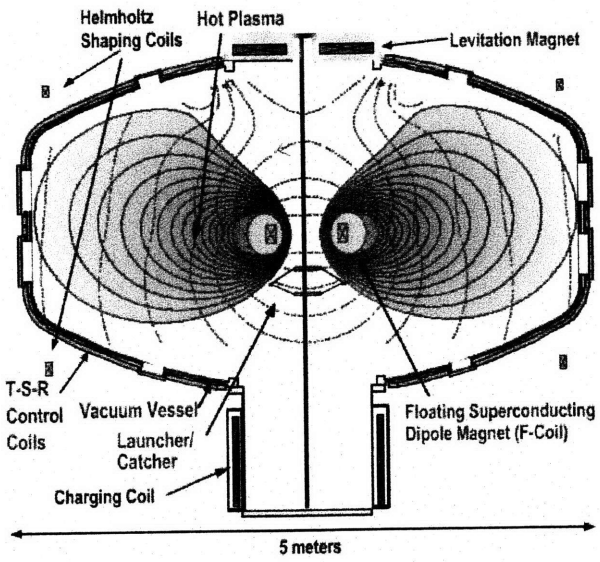

Figures 1.1: Schematic picture of Levitated Dipole Experiment.

LDX is designed for steady state operation in an MHD interchange stable regime[3-6] in the presence of electron cyclotron heating. This heating increases the temperature[7] and introduces a hot electron population. Current experimental measurements suggest that a hot electron population with temperatures in excess of 50 keV and number density of $\sim 3\times 10^{16}\ m^{-3}$ has been achieved while the background plasma is at 10's of eVs with a density of $\sim 1\times 10^{17}\ m^{-3}$.

The presence of these hot electrons can alter plasma stability, leading to the motivation of this work, which is to study the effects of hot electrons on the stability of plasma confined by closed magnetic field lines such as those in dipole geometry. The current work develops a theoretical approach to examining the problem of plasma stability in the presence of a hot species by highlighting many of the key physics issues and by employing a technique that can be used in numerical extensions. To make the analysis analytically tractable to the extent possible, we model the plasma as having an ideal MHD background consisting of ions and electrons plus a

fully kinetic population of hot electrons. To simplify the gyrokinetic hot electron response only a Maxwellian unperturbed distribution function is considered.

It is particularly important to examine the role the hot electrons play in modifying the usual ideal MHD interchange stability condition including wave-particle resonance effects. Based on current LDX experimental observations, unstable modes with frequencies ranging from two to five of kHz to hundreds of MHz are being observed, corresponding to typical magnetic drift frequencies of the background species and hot electrons, respectively. To concentrate on the role the hot electrons play in modifying the interchange stability, we consider modes with wave frequencies much higher than the background and lower or on the same order as the hot species drift frequencies.

Geometrical effects are known to complicate the analysis, so we begin by considering the simplest closed field line geometry, namely, the Z pinch, which is investigated in Chapter 2. It can be thought of as a cylindrical approximation to a general dipole, so that the unperturbed magnetic field is constant and closed on the cylindrical flux surfaces, and the unperturbed diamagnetic current is along the axial direction. It lacks the geometrical details associated with field line averages of quantities, but is useful to help understand the physics behind the driving forces for instability. This simple model also allows us treat the diamagnetic and magnetic drifts as comparable as they are in a dipole and makes it possible to perform a kinetic treatment of the hot electron population in the limit in which the wave frequency resonates with the magnetic drift frequency to cause a destabilizing Landau-type resonance. When the superconducting coil is fully levitated, it is expected to confine plasmas in which the magnetic pressure is comparable to both the background kinetic pressure and the hot electron kinetic pressure. So in our analysis we consider the case when the background kinetic pressure and the hot electron kinetic pressure are

of the same order. However, the experimental measurements of the current LDX plasmas suggest that the plasma pressure is primarily contained in the hot species, presumably because of background plasma losses to the supports of the superconducting coil. To investigate stability in this case, we allow the hot electron pressure to be much higher than the pressure of the background plasma.

We note that the stability analysis presented here is completely different from those employed for a bumpy torus where a hot electron ring is necessary to provide stability in the otherwise unstable mirror cells linked to form a torus[8]. In a Z pinch model of a dipole, stability in the absence of hot electrons is assured by employing a pressure profile that decreases slowly enough to satisfy the usual MHD interchange condition which arises due to the stabilizing influence of plasma and magnetic compressibility in closed magnetic field lines. The hot electrons generated by electron cyclotron heating must then be investigated to determine if they can act in a destabilizing manner. In particular, the curvature and grad B drift must be treated on equal footing. These drifts allow a strongly unstable hot electron drift resonance to occur when the grad B drift opposes the curvature drift. Weaker destabilization occurs when the drifts are in the same direction. Here we remark that high mode number Z pinch interchange stability in the presence of a hot electron population is in some details related to the low mode number alpha particle driven internal kink mode and fishbone instabilities in tokamaks. For these alpha particle driven modes the details of the resonance of the wave with the magnetic drift of the alphas can have a important impact, with drift reversal at some radius leading to instability[9]. In our Z pinch model we are able to investigate the resonant particle mechanism in a simpler geometry that allows us to give a physical interpretation of the effect of drift reversal, which occurs at some critical pitch angle (that is allowed to vary radially). These hot electron drift resonance effects

are considered in detail in Sec. 2.4. In the electrostatic limit when the wave and drift frequencies are comparable our results include the standard hot electron interchange if hot electron temperature gradients are ignored and the hot electron density falls off radially[10].

To examine the role geometrical effects play in the interchange stability of plasma, we expand the Z-pinch calculation of Chapter 2 to a more realistic geometry of a general dipole in Chapter 3. Here the unperturbed magnetic field B_0 is purely in the poloidal direction, while the unperturbed diamagnetic current J_0 is toroidal. We again consider flute or interchange modes with wave frequencies intermediate between the background and hot species drift frequencies. We do not address the hot electron interchange, for which the mode frequency is of the order of the typical hot electron drift frequency[15]. As in the previous chapter, the magnetic drift, consisting of comparable grad B and curvature drifts, is treated on equal footing with the diamagnetic drift. We obtain the dispersion relation for arbitrary plasma and hot electron pressures, but then examine three plasma pressure orderings relative to the magnetic pressure: background electrostatic with $\beta_b << \beta_h \sim 1$, electromagnetic with $1 \sim \beta_b << \beta_h$, and electromagnetic with $1 \sim \beta_b \sim \beta_h$. Throughout this chapter, we compare and contrast the results from dipolar geometry to that of the Z-pinch.

Chapter 2

Effects of kinetic hot electrons on the stability of Z-pinch plasma.

2.1 Introduction

The Levitated Dipole Experiment (LDX)[1,2] is designed to operate in an MHD interchange stable regime[3-6]. Electron cyclotron heating is employed to increase the temperature[7] and will introduce a hot electron population that can alter interchange stability. We examine the effects of a hot Maxwellian electron population on interchange stability of Z-pinch plasma to simplify our analysis. We consider a confined plasma having an ideal MHD background consisting of electrons and ions plus a fully kinetic population of hot electrons. Of particular interest is the role the hot electrons play in modifying the usual ideal MHD interchange stability condition by wave-particle resonance effects.

For the Z pinch geometry the unperturbed magnetic field B_0 is constant and closed on the cylindrical flux surfaces and the unperturbed diamagnetic current J_0 is along the axial direction. The Z pinch approximation to a dipole preserves the essential feature of the closed magnetic field lines, but misses the geometrical details associated with field line averages of quantities, so it is only intended to illustrate the key physics. A more realistic dipole equilibrium is required to make quantitative stability predictions. The Z-pinch model also allows us to consider plasmas in which the magnetic pressure is comparable to both the background kinetic pressure and the hot electron kinetic pressure, as well as to treat the diamagnetic and magnetic

drifts as comparable as they are in a dipole. Moreover, it makes it possible to perform a kinetic treatment of the hot electron population in the limit in which the wave frequency resonates with the magnetic drift frequency to cause a destabilizing Landau-type resonance.

In the low wave frequency limit of interest a particularly strong destabilizing hot electron interaction occurs when the hot electron magnetic drift exhibits reversal due to a change in the grad B_0 direction. In the absence of drift reversal a much weaker resonant particle interaction can occur which can destabilize an otherwise stable interchange, with the new stability boundary depending on the details of the hot electron density and temperature, and their profiles. To make the analysis more tractable and highlight the role of the hot electrons, only flute modes are considered with wave frequencies intermediate between the background and hot species drift frequencies. Flute or interchange modes are the least stable modes in the absence of hot electrons[3-6].

In Sec. 2.2 we derive two coupled equations for the ideal MHD background plasma that depend on the perturbed hot electron number density and radial current. These two quantities are then evaluated kinetically in Sec. 2.3 assuming the unperturbed hot electron population is Maxwellian. Section 2.4 combines the results from the two previous sections to obtain the full dispersion relation that is analyzed in detail, including the hot electron drift resonance de-stabilization effects. A simple hard core Z pinch geometry and the case of a "rigid rotor" are discussed in Sec. 2.5. We remark on the stability of the hot electron interchange (HEI) mode in Sec. 2.6 , following a brief discussion of the results in Sec. 2.7.

2.2. Ideal MHD Treatment Of The Background Plasma

In this section we will develop an ideal MHD treatment for the background plasma that permits a hot electron population to be retained. This treatment allows us to derive a perturbed radial Ampere's law and a perturbed quasi-neutrality condition that depend on the perturbed hot electron radial current and density, respectively, which are evaluated in the next section.

We consider the simplest closed field line configuration of cylindrical Z-pinch geometry in which we only allow radial equilibrium variation. The unperturbed magnetic field is in the azimuthal direction and given by $\vec{\mathbf{B}}_0 = B_0(r)\hat{\boldsymbol{\theta}}$, while the unperturbed current is axial and given by $\vec{\mathbf{J}}_0 = J_0(r)\hat{\mathbf{z}}$. Ampere's law requires

$$\mu_0 r J_0 = (rB_0)', \tag{2.1}$$

where a prime is used to denote radial derivatives.

Denoting the total equilibrium pressure by p_0, force balance gives

$$J_0 B_0 = -p_0', \tag{2.2}$$

where the total pressure is the sum of the background pressure, p_{0b} and hot pressure p_{0h}, $p_0 = p_{0b} + p_{0h}$. The background pressure $p_{0b} = p_{0e} + p_{0i}$ is the sum of the background electron pressure $p_{0e} = n_{0e}T_e$ and the ion pressure $p_{0i} = n_{0i}T_i$, where n_{0e}, n_{0i}, T_e, and T_i are the background electron and ion densities and temperatures. The total current is the sum of the background and hot contributions $J_0 = J_{0b} + J_{0h}$ which satisfy the force balance relations $J_{0b}B_0 = -p_{0b}'$ and $J_{0h}B_0 = -p_{0h}'$.

To derive the perturbed equations we linearize the full equations assuming there is no azimuthal variation ($\partial/\partial\theta = 0$) and that the time and axial dependence are of the form $\exp(-i\omega t - ikz)$, with $\mathrm{Im}\,\omega > 0$ for an unstable mode. The background ion flow velocity $\vec{\mathbf{v}}_1$ is written in terms of the displacement $\vec{\xi}$ as $\vec{\mathbf{v}}_1 = -i\omega\vec{\xi}$. Making the usual ideal MHD assumption that the magnetic field moves with the flow, the perturbed electric field $\vec{\mathbf{E}}_1$ is

$$\vec{\mathbf{E}}_1 = i\omega\vec{\xi}\times\vec{\mathbf{B}}_0, \tag{2.3}$$

so that Faraday's law for the perturbed magnetic field $\vec{\mathbf{B}}_1$ becomes

$$\vec{\mathbf{B}}_1 = \nabla\times\left(\vec{\xi}\times\vec{\mathbf{B}}_0\right). \tag{2.4}$$

Knowing $\vec{\mathbf{B}}_1$, the total perturbed current $\vec{\mathbf{J}}_1 = \vec{\mathbf{J}}_{1b} + \vec{\mathbf{J}}_{1h}$ is evaluated from Ampere's law,

$$\mu_0\vec{\mathbf{J}}_1 = \nabla\times\vec{\mathbf{B}}_1. \tag{2.5}$$

We consider flute modes so Eq. (2.4) gives $B_{1r} = 0 = B_{1z}$ and then Eq. (2.5) requires the parallel current to vanish ($J_{1\theta} = 0$).

To determine the displacement we employ momentum conservation for the background plasma by accounting for the charge imbalance – or uncovering – due to the hot electrons:

$$-m_i n_{0i}\omega^2\vec{\xi} = en_{0h}\vec{\mathbf{E}}_1 + \vec{\mathbf{J}}_{1b}\times\vec{\mathbf{B}}_0 + \vec{\mathbf{J}}_{0b}\times\vec{\mathbf{B}}_1 - \nabla p_{1b}, \tag{2.6}$$

where quasi-neutrality for singly charged ions requires $n_{0h} = n_{0i} - n_{0e}$ and m_i denotes the mass of the background ions. The perturbed pressure of the background plasma p_{1b} is assumed to satisfy an adiabatic equation of state

$$p_{1b} = -\gamma p_{0b}\nabla\cdot\vec{\xi} - p'_{0b}\xi_r, \tag{7}$$

where $\gamma = 5/3$ and ξ_r is the radial component of $\vec{\xi}$.

Using the preceding system of equations, it is convenient to obtain two coupled equations for the azimuthal component of $\vec{\mathbf{B}}_1$ and the radial component of $\vec{\xi}$, that only require knowledge about the perturbed hot electron density and radial current which are evaluated in Sec. III. To carry out this simplification we first define the flux tube volume $V \equiv \oint dl / B_0 = 2\pi r / B_0$ and then form the $\hat{\theta}$ component of Eq. (2.4) to obtain

$$B_{1\theta} = \frac{V'}{V} B_0 \xi_r - B_0 \nabla \cdot \vec{\xi}, \tag{2.8}$$

with $V'/V = 1/r - B_0'/B_0$. Another useful expression is obtained from the radial component of Ampere's law, $ikB_{1\theta} = \mu_0 (J_{1br} + J_{1hr})$, by using the axial component of the momentum equation

$$-m_i n_{0i} \omega^2 \xi_z = e n_{0h} E_{1z} + B_0 J_{1br} + ikp_{1b}$$

to determine J_{1br}, then using Eq. (2.7) and the axial component of (2.3) to eliminate p_{1b} and $E_{1z} = i\omega B_0 \xi_r$, and finally using

$$\nabla \cdot \vec{\xi} = \frac{1}{r} \frac{\partial}{\partial r} (r\xi_r) - ik\xi_z \tag{2.9}$$

to eliminate ξ_z. Defining the background plasma beta by

$$\beta_b \equiv \frac{2\mu_0 p_{0b}}{B_0^2}, \tag{2.10}$$

the resulting equation can be written as

$$B_{1\theta} = \frac{\mu_0 J_{1hr}}{ik} + \frac{\beta_b B_0}{2} \left\{ \gamma \nabla \cdot \vec{\xi} + \left(\frac{p_{0b}'}{p_{0b}} - \frac{\omega e B_0 n_{0h}}{k p_{0b}} \right) \xi_r - \frac{\omega^2 m_i n_{0i}}{k^2 p_{0b}} \left[\nabla \cdot \vec{\xi} - \frac{1}{r} \frac{\partial}{\partial r} (r\xi_r) \right] \right\}. \tag{2.11}$$

If we neglect the coupling to sound waves by assuming $\omega^2 / k^2 << p_{0b} / m_i n_{0i}$, use Eq. (2.8) to eliminate $\nabla \cdot \vec{\xi}$, write ξ_r in terms of the axial electric field E_{1z}, and define the interchange parameter

$$d = -\frac{Vp'_{0b}}{V'p_{0b}} \tag{2.12}$$

and Maxwellian averaged background electron curvature and total magnetic drift frequencies

$$\omega_{\kappa e} = \frac{kT_e}{erB_0} \text{ and } \omega_{de} = \omega_{\kappa e}\frac{rV'}{V}, \tag{2.13}$$

we obtain from Eq. (2.11) the first of the desired equations, the radial Ampere's law, in the form:

$$\left(1+\tfrac{1}{2}\gamma\beta_b\right)\frac{B_{1\theta}}{B_0} = \frac{\mu_0 J_{1br}}{ikB_0} + \frac{\beta_b}{2}\left[(\gamma-d)\frac{\omega_{de}}{\omega} - \frac{n_{0h}T_e}{p_{0b}}\right]\left(\frac{eE_{1z}}{ikT_e}\right). \tag{2.14}$$

To obtain the second equation we start with background charge conservation $\nabla\cdot\vec{\mathbf{J}}_{1b} = i\omega e(n_{1i}-n_{1e})$ and use perturbed quasi-neutrality $n_{1h} = n_{1i} - n_{1e}$ to write

$$i\omega e n_{1h} = \nabla\cdot\vec{\mathbf{J}}_{1b}. \tag{2.15}$$

The interchange assumption means that only the perpendicular component of $\vec{\mathbf{J}}_{1b}$ matters in Eq. (2.15). Solving the momentum equation for $\vec{\mathbf{J}}_{1b\perp}$ by making sure to retain the inertial term in J_{1bz} but continuing to ignore it in J_{1br} to be consistent with the neglect of sound waves in Eq. (2.11)), and inserting the result into Eq. (2.15), gives

$$i\omega e\left[n_{1h} + \left(n'_{0h} + \frac{\omega k n_{0i} m_i}{eB_0}\right)\xi_r + n_{0h}\nabla\cdot\vec{\xi}\right] = -ik\left(\frac{p_{1b}V'}{B_0 V} + \frac{p'_{0b}B_{1\theta}}{B_0^2}\right).$$

Using Eqs. (2.7) and then (2.8) to eliminate p_{1b} and then $\nabla\cdot\vec{\xi}$, writing ξ_r in terms of E_{1z}, using definitions (2.12) and (2.13), and defining $\Omega_i = eB_0/m_i$ and

$$b = \frac{k^2 T_e}{m_i\Omega_i^2}\frac{n_{0i}T_e}{p_{0b}}, \tag{2.16}$$

the preceding gives the quasi-neutrality equation, to be

$$\frac{n_{1h}T_e}{p_{0b}} + \left[b + \frac{\omega_{de}}{\omega}\frac{n_{0h}T_e}{p_{0b}}\left(1 + \frac{rn'_{0h}/n_{0h}}{rV'/V}\right) - \frac{\omega_{de}^2}{\omega^2}(\gamma-d)\right]\left(\frac{eE_{1z}}{ikT_e}\right) = \frac{B_{1\theta}}{B_0}\left[\frac{n_{0h}T_e}{p_{0b}} - \frac{\omega_{de}}{\omega}(\gamma-d)\right]. \tag{2.17}$$

Combining Eqs. (2.14) and (2.17) in the absence of hot particles we recover the usual arbitrary β_b ideal MHD interchange condition[5] in the form

$$\left(\frac{\omega}{\omega_{\kappa e}}\right)^2 = \left(\frac{rV'}{V}\right)^2 \frac{(\gamma-d)}{b}\frac{(2+d\beta_b)}{(2+\gamma\beta_b)}. \tag{2.18}$$

Notice that since our MHD treatment requires $b<<1$ and we are interested in $d\sim 1$, the frequency range of interest is $\omega >> \omega_{\kappa e}$ as assumed. The same coupled system of equations (2.14) and (2.17) can also be obtained kinetically following a procedure which assumes the transit frequency is much greater than the collision frequency which is much greater than the wave, magnetic drift and diamagnetic frequencies[11]. To analyze the modifications due to a Maxwellian hot electron population, n_{1h} and J_{1hr} are calculated kinetically in the next section.

2.3. Kinetic Treatment Of The Hot Electrons

To complete our description we need to kinetically evaluate the perturbed hot electron density and radial current contribution to the Ampere's law and quasi-neutrality equations (2.14) and (2.17). The hot electron response must be evaluated kinetically since the temperature of the hot electron population, T_h, is assumed to be much larger that the background temperatures. As a result, the magnetic drift and diamagnetic frequencies of the hot electrons will be assumed to be much larger than the wave frequency.

We assume that the hot electrons satisfy the Vlasov equation. We then linearize by assuming the unperturbed hot electron distribution function, f_{0h}, is a hot Maxwellian plus a diamagnetic correction:

$$f_{0h} = f_{Mh} - \Omega_e^{-1}\vec{v}\times\hat{\theta}\cdot\nabla f_{Mh}, \tag{2.19}$$

where $f_{Mh} = n_{0h}(m_e/2\pi T_h)^{3/2}\exp\left(-mv^2/2T_h\right)$ and $\Omega_e = eB_0/m_e$, with m_e the electron mass.

The gyro-kinetic equation for the linearized hot electron distribution function f_{1h} is most conveniently rewritten by introducing the scalar and vector potentials via $\vec{\mathbf{E}}_1 = -\nabla\Phi - \partial\vec{\mathbf{A}}/\partial t$ and $\vec{\mathbf{B}}_1 = \nabla\times\vec{\mathbf{A}}$, extracting the adiabatic response by letting

$$f_{1h} = \frac{e\Phi}{T_h} f_{Mh} + g e^{iL}, \tag{2.20}$$

where $L = \Omega_e^{-1}\vec{\mathbf{k}}\cdot\vec{\mathbf{v}}\times\hat{\boldsymbol{\theta}}$ and $\vec{\mathbf{v}} = \mathrm{v}_\perp(\hat{\mathbf{z}}\cos\theta + \hat{\mathbf{r}}\sin\theta) + \mathrm{v}_\parallel\hat{\boldsymbol{\theta}}$, and then seeking solutions of the form $\exp(-i\omega t - iS)$ where $\nabla S = \vec{\mathbf{k}}_\perp$. The resulting gyro-kinetic equation for g becomes[12,13]

$$-i(\omega - \vec{\mathbf{k}}\cdot\vec{\mathbf{v}}_{dh})g = i\frac{e}{T_h} f_{Mh}\left(\omega - \omega_{*h}^T\right)\left[(\Phi - \mathrm{v}_\parallel A_\theta)J_0(a_h) - \frac{\mathrm{v}_\perp B_{1\theta}}{k_\perp}J_1(a_h)\right], \tag{2.21}$$

where $J_0(a_h)$ and $J_1(a_h)$ are Bessel functions of the first kind with $a_h = k_\perp \mathrm{v}_\perp/\Omega_e$. In Eq. (2.21)

$$\vec{\mathbf{k}}\cdot\vec{\mathbf{v}}_{dh} = \frac{k}{r\Omega_e}\left(\mathrm{v}_\parallel^2 - \mathrm{v}_\perp^2\frac{rB_0'}{2B_0}\right) = \omega_{\kappa h}\frac{m\mathrm{v}^2}{2T_h}\left[(1+s)\lambda^2 + (1-s)\right] \tag{2.22}$$

is the grad B_0 plus curvature magnetic drift frequency with $\omega_{\kappa h} = kT_h/erB_0$ the curvature drift frequency, $\lambda = \mathrm{v}_\parallel/\mathrm{v}$ a pitch angle variable and

$$s \equiv 1 + \frac{rB_0'}{B_0}, \tag{2.23}$$

where $s = 0$ corresponds to the vacuum limit. In addition,

$$\omega_{*h}^T = \omega_{*h}\left[1 + \eta_h\left(\frac{m\mathrm{v}^2}{2T_h} - \frac{3}{2}\right)\right] \tag{2.24}$$

is the hot electron diamagnetic drift frequency with $\eta_h = (T_h'/T_h)/(n_{0h}'/n_{0h})$ and

$$\omega_{*h} = -\frac{kT_h n_{0h}'}{eB_0 n_{0h}}. \tag{2.25}$$

The $v_{\|}/\left(\omega-\vec{k}\cdot\vec{v}_{dh}\right)$ moment of the gyro-kinetic equation (2.21) shows that $J_{1\theta h}$ is proportional to A_θ. Moreover, as mentioned earlier, there is no perturbed parallel current carried by the background plasma. As a result, the parallel component of the Ampere's law results in a homogeneous equation for A_θ. Therefore, we may safely assume $A_\theta = 0$ and $\vec{B}_1 = B_{1\theta}\hat{\theta}$, consistent with Eq. (2.4) and our interchange assumption. In addition, we assume that axial wavelengths are much shorter than azimuthal wavelengths and radial derivatives of unperturbed quantities. Consequently, $k_\perp \approx k$, $L \approx k v_\perp \Omega_e^{-1} \sin\theta$ and $a_h \approx k v_\perp / \Omega_e$ may be employed. Finally, we allow the hot to background temperature ratio to be as large as $T_h / T_e \sim m_i / m_e$ so that $a_h^2 \sim b << 1$ and $L << 1$. Then we may use $J_0 \approx 1$, $J_1 \approx a_h / 2$, and $\exp(iL) \approx 1 + iL$ to reduce Eqs. (2.20) and (2.21) to

$$f_{1h} \approx f_{Mh}\left[\frac{e\Phi}{T_h} - \left(\frac{\omega - \omega_{*h}^T}{\omega - \vec{k}\cdot\vec{v}_{dh}}\right)\left(\frac{e\Phi}{T_h} - \frac{m v_\perp^2 B_{1\theta}}{2 T_h B_0}\right)(1+iL)\right]. \tag{2.26}$$

To simplify our calculations, we note that our short axial wavelength assumption along with the Coulomb gauge $\nabla\cdot\vec{A} = 0$ implies that $A_z << A_r$. As a result, $E_{1z} \approx ik\Phi$ may be employed to make the replacement

$$\frac{eE_{1z}}{ikT_e} \approx \frac{e\Phi}{T_e}. \tag{2.27}$$

in the perturbed radial Ampere's law, Eq. (2.14), and quasi-neutrality condition, Eq. (2.17). If the assumption of $\beta_b \sim 1$ is made, these equations also imply the ordering

$$\frac{B_{1\theta}}{B_0} \sim \frac{e\Phi\omega_{\kappa e}}{T_e\omega} = \frac{e\Phi\omega_{\kappa h}}{T_h\omega}. \tag{2.28}$$

To simplify the results for the hot electrons while maintaining $T_h >> T_e$ we will assume $\omega_{\kappa h} >> \omega >> \omega_{\kappa e}$ and thus

$$\frac{T_h}{T_e} >> \frac{\omega}{\omega_{*e}} >> 1. \tag{2.29}$$

Keeping the above simplifications in mind, we can integrate the distribution function, Eq. (2.26), over velocity space and obtain perturbed hot electron density, $n_{1h} = \int f_{1h} d\vec{v}$, and radial current, $J_{1hr} = -e\int v_r f_{1h} d\vec{v}$. Fortunately, the full expressions for n_{1h} and J_{1hr} will not be required. Only the approximations given in the Appendix 2.A are needed. For the moment we need only define the hot electron beta

$$\beta_h = \frac{2\mu_0 p_{0h}}{B_0^2} \quad \text{and} \quad s_h = -\frac{\beta_h}{2}\frac{rp'_{0h}}{p_{0h}},$$

and comment that the expressions in the Appendix 2.A lead to the forms:

$$\frac{n_{1h}}{n_{0h}} = \frac{e\Phi}{T_h} G + \frac{B_{1\theta}}{B_0} H \quad \text{and} \quad \frac{\mu_0 J_{1hr}}{ikB_0} = \frac{e\Phi}{T_h}\frac{\beta_h}{2} H - \frac{B_{1\theta}}{B_0} s_h I, \tag{2.30}$$

where $H \sim G \sim s_h I \sim 1$, except in the vicinity of $s = 1$, where $H \sim G \sim s_h I \sim \sqrt{\omega_{*h}/\omega}$. We remark that even though $\omega_{*h} >> \omega$, it is important to keep the ω term in the denominator of the f_{1h} expression to resolve singularities during the evaluation of the integrals.

2.4 Dispersion Relation

Combining the perturbed radial Ampere's law, Eq. (2.14), and quasi-neutrality condition, Eq. (2.17), with the expressions for n_{1h} and J_{1hr} from the previous section, we can form the dispersion relation, which can be written as

$$\begin{aligned} &\left\{ b + \frac{\omega_{de}^2}{\omega^2}(d-\gamma) + \frac{n_{0h}T_e}{p_{0b}}\left[\frac{T_e}{T_h}G + \frac{\omega_{de}}{\omega}\left(1 + \frac{rn'_{0h}/n_{0h}}{rV'/V}\right)\right]\right\}\left(1 + \frac{1}{2}\gamma\beta_b + s_h I\right) + \\ &+ \frac{\beta_b}{2}\left[\frac{\omega_{de}}{\omega}(d-\gamma) + \frac{n_{0h}T_e}{p_{0b}}(1-H)\right]^2 = 0 \end{aligned} \tag{2.31}$$

If we consider comparable hot electron pressure and background pressure then in the absence of the finite Larmor radius term b, Eq. (2.31) is seen to permit only solutions with $\omega_{de}/\omega \sim n_{0h}/n_{0i}$ since we order $d \sim \beta_b \sim \beta_h \sim s_h I \sim G \sim H \sim V n_{0h}'/n_{0h}V'$ for the case of $s \neq 1$. Therefore, the neglect of b violates the ordering imposed by Eq. (2.29) when $\beta_b \sim \beta_h$. Consequently we proceed for now by assuming $b \sim \omega_{\kappa e}^2/\omega^2 >> (n_{0h}/n_{0i})^2$ and neglecting order $n_{0h}/n_{0i} \sim T_e/T_h$ terms compared to $\omega_{\kappa e}/\omega$ in the dispersion relation. For the case of $s \neq 1$ this assumption corresponds to neglecting G and H as well as the equilibrium hot electron density gradient term. Thus, the only hot electron contribution that matters in Eq. (2.31) is $s_h I$ and the dispersion relation then reduces to

$$\frac{\omega^2}{\omega_{\kappa e}^2} = \left(\frac{rV'}{V}\right)^2 \frac{(\gamma - d)}{b} \frac{\left(1+\frac{1}{2}d\beta_b + s_h I\right)}{\left(1+\frac{1}{2}\gamma\beta_b + s_h I\right)}. \tag{2.32}$$

Had we retained finite hot electron gyro-radius terms they would have entered as small order a_h^2 corrections to $s_h I$ in Eq. (2.32).

To evaluate I we only need the lowest order expression for J_{1hr}:

$$\frac{\mu_0 J_{1hr}}{ikB_0} \approx -\frac{\beta_h B_{1\theta}\omega_{*h}}{\sqrt{\pi}B_0\omega_{\kappa h}} \int_0^\infty dt e^{-t^2} t^4 \left[1 + \eta_h\left(t^2 - \frac{3}{2}\right)\right] \int_{-1}^{1} \frac{d\lambda\left(1-\lambda^2\right)^2}{D - \omega/\omega_{\kappa h}t^2} = -\frac{B_{1\theta}}{B_0} s_h I, \tag{2.33}$$

where $t^2 = mv^2/2T_h$ and $D = (1+s)\lambda^2 + (1-s)$. To perform the integral in I for $k > 0$ we may neglect the ω term by using $\omega << \omega_{\kappa h}$ in the denominator except (i) in the vicinity of $s = 1$ and (ii) to insure the path of integration is on the causal side of the $D = 0$ singularity for $s > 1$. The sign of the imaginary part of I for $s > 1$ changes if $k < 0$. Recall that reality requires $-\omega^*, -k$ to be a solution if ω, k is a solution so hereafter we will only consider $k > 0$. Leaving the details of this calculation to the Appendix 2.A, we find that we can write the expression for I as

$$I \approx \begin{cases} -\frac{1}{(1+s)^2}\left((s+4)+\frac{3}{\sqrt{s^2-1}}\ln\left(s+\sqrt{s^2-1}\right)-\frac{3\pi i}{\sqrt{s^2-1}}\right) & s>1 \\ -\left[\frac{5}{4}-i\sqrt{\frac{\omega_{\kappa h}}{\omega}}\frac{\sqrt{2\pi}\left(1+\frac{3}{2}\eta_h\right)}{(1+\eta_h)}\right] & s=1 \\ -\frac{1}{(1+s)^2}\left((s+4)-\frac{6}{\sqrt{1-s^2}}\arctan\sqrt{\frac{1+s}{1-s}}\right) & -1<s<1. \\ \frac{2}{5} & s=-1 \\ -\frac{1}{(1+s)^2}\left((s+4)-\frac{3}{\sqrt{s^2-1}}\ln\left(-s+\sqrt{s^2-1}\right)\right) & s<-1 \end{cases} \qquad (2.34)$$

Expressions for I in the vicinity of $s=1$ are given in the Appendix 2.A for completeness. We remark that our analysis ignores drift resonances of the background species since they are exponentially small and of order $\exp(-\omega/\omega_{\kappa e})$, where $\omega >> \omega_{\kappa e}$.

Notice that for $s>1$ a large imaginary term enters because of the vanishing of the hot electron drift velocity for some pitch angle. This singularity in the drift introduces a Landau resonance in pitch angle space between the wave and the drifting hot electrons. The effective dissipation associated with the vanishing of the hot electron drift resonance makes it such that one root will be unstable because there will always be a sign of k for which $\mathrm{Im}\,\omega>0$. Before examining the $s<1$ case in detail we discuss the physical mechanism responsible for instability when $s \lesssim 1$.

The Landau resonance between the wave and the hot electron magnetic drift has two different forms. When $s<1$ the hot electron magnetic drift does not reverse and the wave-particle interaction is weak because the wave frequency is much smaller than the hot electron drift frequency except for a very low speed hot electrons. That is $\omega=\vec{\mathbf{k}}\cdot\vec{\mathbf{v}}_{dh}$ can only be satisfied if v is very small since the surfaces of constant $\vec{\mathbf{k}}\cdot\vec{\mathbf{v}}_{dh}$ are closed ellipses about $\mathrm{v}=0$ in the $\mathrm{v}_{\|},\mathrm{v}_{\perp}$ plane. As s approaches unity the ellipse opens and becomes hyperbolic because

the drift frequency reverses. A stronger interaction occurs for $s \geq 1$ because particles of all speed are resonant near the critical pitch angle. For $s > 1$ the hot electrons with smaller pitch angles drift along the positive z axis while the larger pitch angle ones continue to drift in the negative z direction (as for $s < 1$). The energy exchange with the near stationary wave is strong since many more hot electrons are involved in the resonant interaction.

2.4.A. Strong resonant hot electron case ($s \geq 1$).

For the special case $s = 1$ there is only curvature drift and all hot electrons are drifting in the same direction along the negative z axis. Energy flows from these particles to the nearly stationary growing wave since all the particles are moving faster than the wave and are therefore being slowed by it. As s increases above unity the drift direction of the lower pitch angle hot electrons reverse and these hot electrons moving slower than the wave are able to extract energy from it so the growth rate decreases. The wave remains unstable, however, and the parabolic dependence of the magnetic drift on pitch angle, $\vec{\mathbf{k}} \cdot \vec{\mathbf{v}}_{dh} \propto \lambda^2 - \lambda_0^2$ with $\lambda_0^2 = (s-1)/(s+1)$ means that for s>1 there is always a critical pitch angle λ_0 for destabilization. The $s > 1$ case is always unstable since the hot electrons with pitch angles above the critical pitch angle for drift reversal, λ_0, are always able to give more energy to the wave than those below λ_0, which extract it from the wave.

If the Maxwellian hot electron distribution function were replaced by a bi-Maxwellian with $T_{\perp h} > T_{\parallel h}$ then there would be fewer faster and more slower hot electrons near λ_0. The growth rate for $s > 1$ would decrease. However, the sign of the residue would not change

because, unlike standard Landau damping, drift resonance Landau damping depends on ω_h^T, rather than on the velocity space derivative of f_{0h}, as can be seen in Eq. (2.26). Because $\omega << \omega_{\kappa h}$, the wave is essentially stationary and simply a means of transferring energy between the counter drifting hot electrons so ω may safely be neglected in the expressions for I (except near $s=1$ where I depends on ω because there are few if any drift reversed particles). Only in the limit $s \to \infty$, when the drifts of all hot electrons are reversed does the resonant drive vanish for $s \geq 1$.

The special case $rV'/V = 2 - s \to 0$ corresponds to $B_0 \propto r$ (flux tube volume independent of r), but since $d \propto V/rV' \to \infty$ it is always unstable even in the absence of hot electrons as can be seen from Eq. (2.32). The growth rate ($\mathrm{Im}\,\omega$) for other $s>1$ can be estimated from Eqs. (2.32) and (2.34) to find

$$\mathrm{Im}\,\omega/\omega_{\kappa e} \sim \frac{\beta_h \beta_b |\gamma - d|^{3/2} |2-s| (rp'_{0h}/p_{0h})}{(1+s)^2 \sqrt{b(s^2-1)}} \tag{2.35}$$

for $\beta_b \sim d \sim 1$. Notice that the growth rate vanishes for $d = \gamma$ and/or $s \to \infty$.

2.4.B. Weak resonant hot electron case ($s<1$).

For $s<1$ the stable operating regime of most interest satisfies the usual interchange stability condition $\gamma > d$ along with the additional condition $1 + \beta_b d/2 + s_h I > 0$. To better understand this regime it is convenient to write equilibrium force balance in terms of s as

$$s = s_h - \beta_b \frac{rp'_{0b}}{2p_{0b}}.$$

Then d can be written in terms of s and s_h as

$$1+\tfrac{1}{2}\beta_b d=\tfrac{2-s_h}{2-s}. \tag{2.36}$$

Using this result, $\gamma > d$ becomes

$$s_h > -\gamma\beta_b + \left(1+\tfrac{1}{2}\gamma\beta_b\right)s. \tag{2.37}$$

Then, ignoring for the moment resonant particles effects for $s<1$, the stability condition of Eq. (2.32) can be illustrated graphically by plotting s_h as a function of s for a given value of background beta as shown in Figs. 2.1.

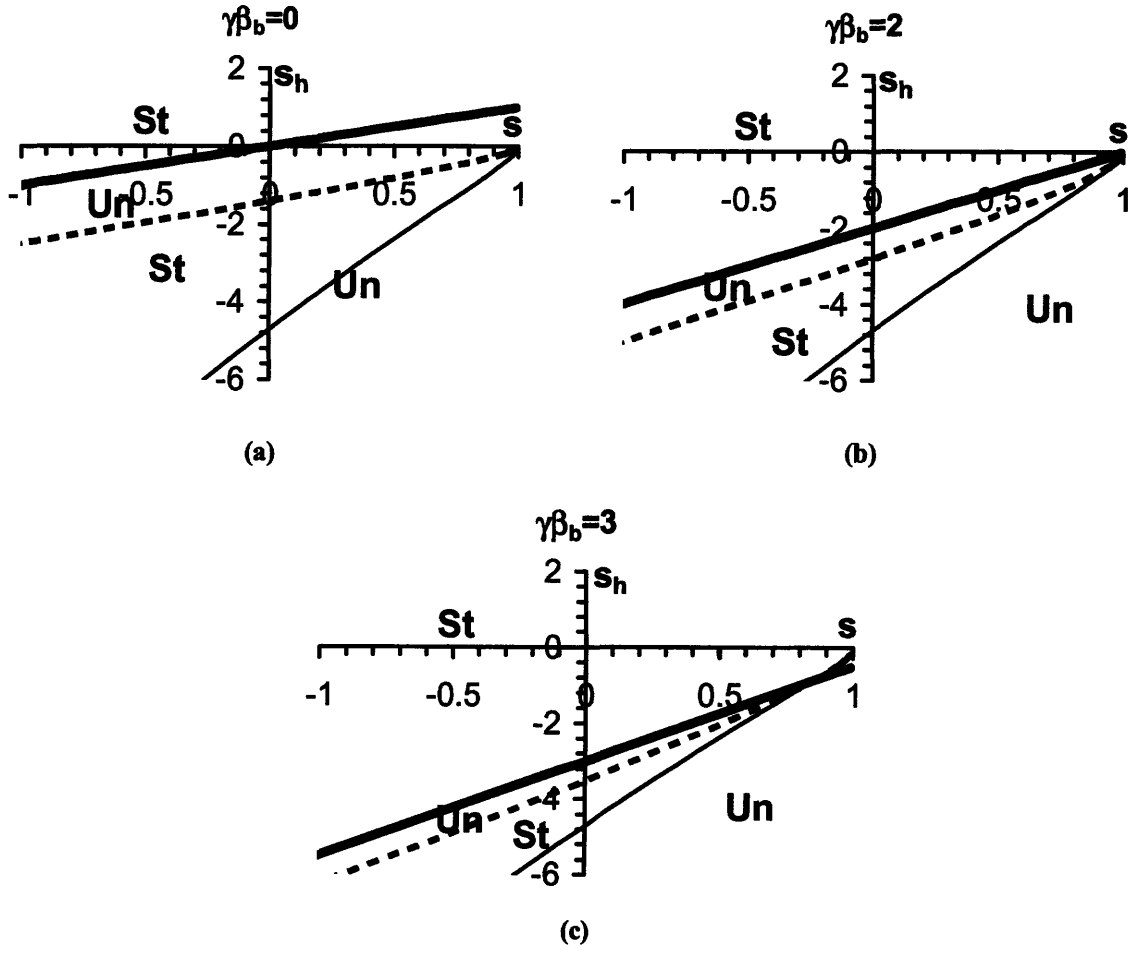

Figures 2.1 (a)-(c): Stability regions for different values of $\gamma\beta_b$ with b=0.01 and $n_{0h}T_e/p_{0b}$=5%. The bold solid line is γ=d, the thin solid line is $1+d\beta_b/2+s_hI=0$, and the dotted is $1+\gamma\beta_b/2+s_hI=0$. St and Un indicate stable and unstable regions.

Notice that when the hot electrons are ignored, i.e. $s_h = 0$, we recover the usual Z-pinch stability condition[14], $s < \gamma\beta_b/(1+\gamma\beta_b/2)$. The plots also show that the β_b term increases the size of the stable region, allowing more general hot pressure profiles (i.e. s_h can be negative as well as positive for $s = 0$). However, as $s \to 1$, I becomes large, so the curves $1 + d\beta_b/2 + s_h I = 0$ and $1 + \gamma\beta_b/2 + s_h I = 0$, which cross at $d = \gamma$, require $s_h \to 0$ at $s = 1$. To prevent a sign change in Eq. (2.32) we need to be above all three curves to maintain stability. From plots like Figs. 2.1 we can see that a value of $\gamma\beta_b$ between about 3 and 5 optimizes the stable operating region since a larger β_b does not substantially increase the stable operating regime.

So far we have assumed $|rn'_{0h}/n_{0h}| \sim 1$ and thus, due to Eq. (2.29), were able to neglect terms that involve hot electron density gradient. However, it is possible to have a steeper hot electron density gradient – so steep that $|rn'_{0h}/n_{0h}| >> 1$. If we assume that the hot electron temperature and density profiles are similar and consider a smooth profile for equilibrium background pressure, then $|rn'_{0h}/n_{0h}| \sim |s_h| \sim |s|$ due to equilibrium force balance, $s = -\beta_b r p'_{0b}/2p_{0b} + s_h$. However the hot electron density gradient only enters in the form $(rn'_{0h}/n_{0h})/(2-s)$, which for $|rn'_{0h}/n_{0h}| >> 1$ is of order unity. Thus because of the direct relation between $|rn'_{0h}/n_{0h}|$ and $|s|$ through the equilibrium force balance and the ordering imposed by Eq. (2.29), the hot electron density gradient terms do not become significant enough to appear in the dispersion relation.

During the operation of LDX it is anticipated that the hot electron pressure will become much larger than background pressure. Therefore we also consider the case of $\beta_h >> \beta_b$, by

taking $b \sim \omega_{*e}^2/\omega^2 \sim (n_{0h}/n_{0i})^2$. This ordering leads to neglecting only the G term in the lowest order dispersion relation Eq. (2.31), due to the ordering imposed by Eq. (2.29).

As before, the drift reversal case ($s>1$) continues to be strongly destabilizing due to large imaginary terms in I and H. If we ignore weak resonant hot electron effects, the stability condition for $s<1$ case can be written as

$$1+Y \geq 0, \tag{2.38}$$

where to the lowest order we find $H = -\frac{rn'_{0h}}{2n_{0h}} \int_{-1}^{1} \frac{d\lambda(1-\lambda^2)}{(1+s)\lambda^2+(1-s)}$ from Eq. (2.A7), and we define

$$Y = \frac{2(\gamma-d)}{\left(1+\frac{rn'_{0h}/n_{0h}}{rV'/V}\right)^2}\left[\frac{2b}{(n_{0h}T_e/p_{0b})^2}\frac{\left(1+\frac{1}{2}d\beta_b+s_hI\right)}{\left(1+\frac{1}{2}\gamma\beta_b+s_hI\right)} - \frac{\beta_b(1-H)\left(\frac{rn'_{0h}/n_{0h}}{rV'/V}+H\right)}{\left(1+\frac{1}{2}\gamma\beta_b+s_hI\right)}\right].$$

If electrostatic fluctuations are considered ($\beta_b = 0$) this condition reduces to

$$\left(\frac{n_{0h}T_e}{p_{0b}}\right)^2\left(1+\frac{rn'_{0h}/n_{0h}}{rV'/V}\right)^2 + 4b(\gamma-d) \geq 0,$$

from which we can see a tendency for the hot electrons improve lowest order stability by allowing d to be larger than γ since $b>0$.

Examining the full expression for $Y+1$ we see that when $\beta_b \to 0$, $Y >> 1$. As a result, the stability boundaries are the same as in Fig. 2.1(a) for this limit. For other values of β_b, the stability regions can be plotted as shown in Figs. 2.2 for various values of $\gamma\beta_b$ and rn'_{0h}/n_{0h}. Comparing Figs. 2.2 (a),(b) with Fig. 2.1 (b) and Figs. 2.2 (c),(d) with Fig. 2.1 (c) we can see that the hot electrons somewhat improve the lowest order stability, as in the electrostatic limit.

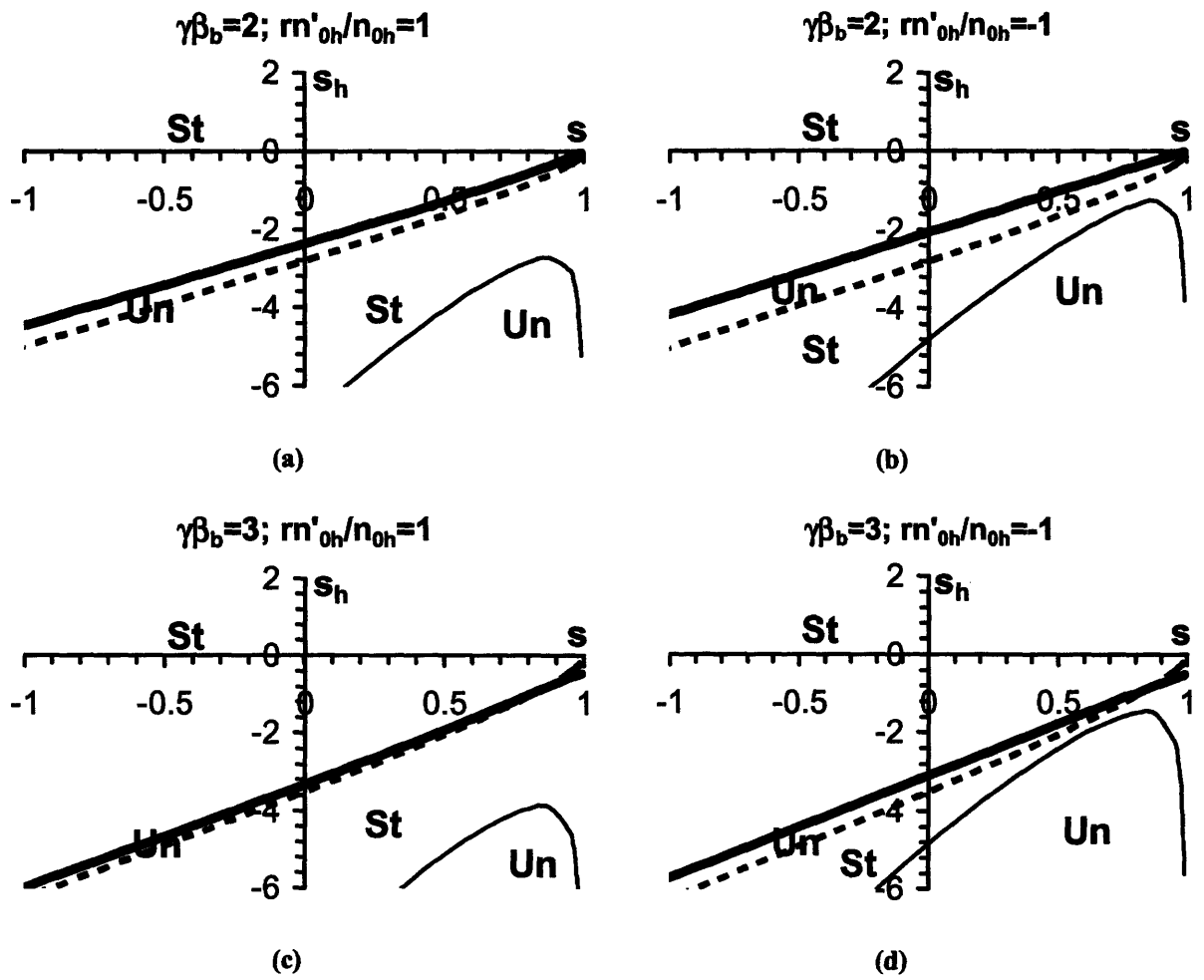

Figures 2.2 (a)-(d): Stability regions for different values of $\gamma\beta_b$ and rn'_{0h}/n_{0h} with b=0.01, $\beta_h=7\beta_b$ and $n_{0h}T_e/p_{0b}=10\%$. The dotted line is the $1+\gamma\beta_b/2+s_hI=0$ curve and for small $\gamma\beta_b$ the bold solid line approaches $\gamma=d$. The thin solid line becomes $1+d\beta_b/2+s_hI=0$ as $n_{0h}\to 0$.

Comparing the plots of Figs. 2.1 and 2.2 we can conclude that stability remains robust even at $\beta_h >> \beta_b$ as long as the region of operation is above the solid curves and the area of drift reversal ($s > 1$) is avoided, with higher hot electron fractions improving stability.

As noted earlier, the resonant hot electron interaction enters as a weaker effect for $s < 1$ than it does for $s > 1$, which is always strongly unstable. We next consider the effect of these resonant hot electrons on stability for $s < 1$ by evaluating their contributions to the perturbed hot

electron density and radial current density for the real part of ω greater than zero ($\mathrm{Re}\,\omega > 0$) as described in the Appendix 2.A:

$$\left.\frac{n_{1h}}{n_{0h}}\right|_{res} = \frac{B_{1\theta}}{B_0} H_{res} + \frac{e\Phi}{T_h} G_{res} \text{ and } \left.\frac{\mu_0 J_{1hr}}{ikB_0}\right|_{res} = \frac{e\Phi_1}{T_h}\frac{\beta_h}{2} H_{res} - \frac{B_{1\theta}}{B_0}(s_h I)_{res}, \tag{2.39}$$

where

$$\begin{aligned} G_{res} &= -i\Delta \frac{15\beta_b}{\beta_h}\left(\frac{T_h}{T_e}\right)^2, \\ H_{res} &= -\frac{2\omega_0 G_{res}}{3\omega_{\kappa h}(1-s)} \quad \text{and} \quad (s_h I)_{res} = -\frac{4\beta_h \omega_0^2 G_{res}}{15\omega_{\kappa h}^2 (1-s)^2}, \end{aligned} \tag{2.40}$$

with Δ defined by

$$\Delta = \frac{(2\pi\omega_0)^{1/2}\omega_{*h}\left(1-\frac{3}{2}\eta_h\right)}{15\omega_{\kappa h}^{3/2}(1-s)}\frac{\beta_h}{\beta_b}\left(\frac{T_e}{T_h}\right)^2. \tag{2.41}$$

Here and elsewhere ω_0 is the positive stable root of Eq. (2.31), which can be schematically represented as

$$A\frac{\omega_0^2}{\omega_{de}^2} + B\frac{\omega_0}{\omega_{de}} + C = 0,$$

where A, B and C are coefficients of corresponding powers of ω_0 / ω_{de}.

Retaining the resonant interaction perturbatively in Eq. (2.31) using $\omega = \omega_0 + \omega_1$, with $\omega_0 >> |\omega_1|$ gives

$$\frac{\omega_1}{\omega_0} = i\Delta K F, \tag{2.42}$$

where

$$K = \kappa^2[\alpha(1-H)-1]^2 + 5\kappa[\alpha(1-H)-1] + \frac{15}{2} = \left\{\kappa[\alpha(1-H)-1] + \frac{5}{2}\right\}^2 + \frac{5}{4} > 0, \tag{2.43}$$

which is a strictly positive quantity,

and

$$F=\frac{\left(1+\frac{1}{2}\gamma\beta_b+s_hI\right)}{A+\frac{\omega_{de}}{2\omega_0}B}, \tag{2.44}$$

with

$$\kappa=\frac{\beta_b(\gamma-d)(2-s)}{\left(1+\frac{1}{2}\gamma\beta_b+s_hI\right)(1-s)} \quad \text{and} \quad \alpha=\frac{\omega_0 n_{0h}T_e}{\omega_{de}p_{0b}(\gamma-d)}. \tag{2.45}$$

As a result the sign of ω_1/ω_0 depends the sign of product ΔF.

If we consider comparable background and hot electron pressures ($\beta_h \sim \beta_b$), then the α terms become negligible because using Eq. (2.32) gives $\alpha \sim n_{0h}T_e/\left(p_{0b}\sqrt{b}\right)\ll 1$. After substituting in the expressions $A=b\left(1+\frac{1}{2}\gamma\beta_b+s_hI\right)$, $B=0$ and $C=(d-\gamma)\left(1+\frac{1}{2}d\beta_b+s_hI\right)$ for this limit, we find that $F=1/b$. Equation (2.42) then reduces to

$$\frac{\omega_1}{\omega_0}=\frac{i\Delta}{b}\left[\left(\kappa-\frac{5}{2}\right)^2+\frac{5}{4}\right]. \tag{2.46}$$

As we can see the sign of ω_1/ω_0 depends only on the sign of Δ. As a result, for $\beta_h \sim \beta_b$, a weak instability of the drift resonant hot electrons ($\omega_0>0$) occurs if $\omega_{*h}(1-3\eta_h/2)>0$ or

$$\frac{3}{2}\frac{rT_h'}{T_h}>\frac{rn_{0h}'}{n_{0h}}. \tag{2.47}$$

The analysis of weak resonant hot electrons effects for the case of $\beta_h \gg \beta_b$ is more complicated since the stability is determined by the sign of the product of ΔF. We first observe that we are only interested if the stable operating region above the bold solid curve in Figs. 2.2 can become destabilized by this weak interaction, since the stable region below the bold solid curve does not allow the hot electron pressure to fall off (positive s_h). In the region of interest, above the bold solid curve in Figs. 2.2, the numerator of F is clearly positive, while the denominator is also positive, but for a more subtle reason. Since the negative real roots of the

dispersion relation Eq. (2.31) are always stable in the absence of resonant hot electrons we are only interested in $\omega_0 > 0$. Using our schematic representation of zero order dispersion relation the denominator of F can be rewritten as

$$A + \frac{\omega_{de}}{2\omega_0} B = \pm \frac{\omega_{de}}{2\omega_0} \sqrt{B^2 - 4AC}\,.$$

In the region of interest $A > 0$ and $C < 0$, thus the dispersion relation has two real roots – one positive and one negative. Only the positive root can be unstable for $k > 0$, and it makes the denominator of F positive. Consequently, the sign of ω_1 / ω_0 depends on the sign of Δ, and is therefore given by Eq. (2.47).

Notice that in the electrostatic limit $\beta_b = 0$, $A = b > 0$, $B = (n_{0h} T_e / p_{0b})(1 + d \ln n_{0h} / d \ln V)$, and $C = (d - \gamma)$. In this case $s = s_h$, and as a result, d cannot be determined from Eq. (2.36) and is a free parameter. If $d > \gamma$, then $C < 0$ and the stability of the region depends on the sign of B, since there are two real roots. If $(1 + d \ln n_{0h} / d \ln V) > 0$ then both roots are negative and the region is stable, due to the absence of drift resonance. If $d < \gamma$, $C > 0$ and there is only one positive root in the lowest order stable region. Then the stability is determined by the sign of Δ and therefore by Eq. (2.47). It is also clear that the temperature profile of hot electrons plays an important role in stabilizing this weak drift instability, since if $\eta_h = 0$ only increasing density profiles can be stable. To confirm that this drift resonance driven mode is indeed weak for $s < 1$ we note that $(\omega_0 / \omega_{\kappa e})^2 \sim 1/b$ giving $\omega_1 / \omega_0 \sim (\beta_h / \beta_b)(\omega_0 / \omega_{\kappa h})^{5/2} << 1$ for $\beta_h \sim \beta_b$.

From the overall discussion of stability, we can conclude that while large hot electron density gradient as well as high background beta are beneficial for the zero order stability, they

are destabilizing when the first order correction is considered, particularly if rn'_{0h}/n_{0h} is negative and greater than 2 to 3 in magnitude for $\beta_b \sim 1$. So, to maximize the overall stable region $rn'_{0h}/n_{0h} > -2$, it is best to keep $\gamma\beta_b \sim 2$ and $2 > rn'_{0h}/n_{0h} > 3rT'_h/2T_h$ along with $\gamma > d$.

2.5. Applications

As a specific application of the results obtained in the previous section we consider a hard core Z pinch as a crude approximation to a dipole with a levitated current carrying superconducting coil as in LDX. Assuming power law profiles satisfying pressure balance gives

$$B_0 = B_a\left(\frac{a}{r}\right)^{1/(1+\beta)} \text{ and } p_0 = p_a\left(\frac{a}{r}\right)^{2/(1+\beta)}, \tag{2.48}$$

where a is the radius of the current carrying hard core conductor, B_a and p_a are the magnetic field and total plasma pressure at its surface, respectively, and $\beta = 2\mu_0 p_a / B_a^2$ is the total beta. If we assume that the background and hot pressure profiles are the same, then $p_a = p_{ab} + p_{ah}$ with $p_{ab} \sim p_{ah}$ and

$$p_{0b} = p_{ab}\left(\frac{a}{r}\right)^{2/(1+\beta)} \text{ and } p_{0h} = p_{ah}\left(\frac{a}{r}\right)^{2/(1+\beta)}, \tag{2.49}$$

where $\beta = 2\mu_0(p_{ab} + p_{ah})/B_0^2 = \beta_b + \beta_h$.

For this special model

$$s = -\frac{\beta r p'_0}{2p_0} = \frac{\beta}{(1+\beta)} > 0 \text{ and } s_h = -\frac{\beta_h r p'_{0h}}{2p_{0h}} = \frac{\beta_h}{(1+\beta)} > 0. \tag{2.50}$$

Note that since $s<1$, drift reversal is not possible in this model. The stability condition for a hard core Z-pinch with the above profiles can be obtained by substituting these expressions for s and s_h into the lowest order dispersion relation, Eq. (2.32), to find

$$\frac{\omega^2}{\omega_{ke}^2}=\left(\frac{rV'}{V}\right)^2\frac{(\gamma-d)}{b}\frac{\left(1+\frac{1}{2}d\beta_b+\frac{\beta_h}{1+\beta}I\right)}{\left(1+\frac{1}{2}\gamma\beta_b+\frac{\beta_h}{1+\beta}I\right)}, \tag{2.51}$$

where $d=2/(2+\beta)>0$ and $[1+d\beta_b/2+\beta_h I/(1+\beta)]/[1+\gamma\beta_b/2+\beta_h I/(1+\beta)]>0$ since $I>0$. Therefore, in the absence of resonant hot electron effects the stability boundary is described by

$$\gamma>d=\frac{2}{2+\beta}, \tag{2.52}$$

which is always satisfied.

To determine the stability condition for the case of $\beta_h >> \beta_b$, we assume power law temperature and density profiles

$$T_h=T_{ah}\left(\frac{a}{r}\right)^{q_h/(1+\beta)} \text{ and } n_{0h}=\frac{p_{ah}}{T_{ah}}\left(\frac{a}{r}\right)^{(2-q_h)/(1+\beta)} \tag{2.53}$$

with $0<q_h<2$. Substituting the expressions for s and s_h along with the hot electron number density gradient into Eq. (2.38), we find the stability condition to be the same as in the $\beta_h \sim \beta_b$ case. For $\beta_b \to 0$ Eq. (2.38) is satisfied since $1+Y>0$. For the case of $\beta_b \neq 0$, Y is smallest if $b=0$. Moreover, a plot of $1+Y$ as a function of β_b/β in Fig. 2.3 for different values of q_h and $\gamma\beta_b=3$ always finds $1+Y>0$. For other values of $\gamma\beta_b$ the plots look very similar to Fig. 2.3 and thus, even for the worst case of $b=0$, Eq. (2.38) is satisfied.

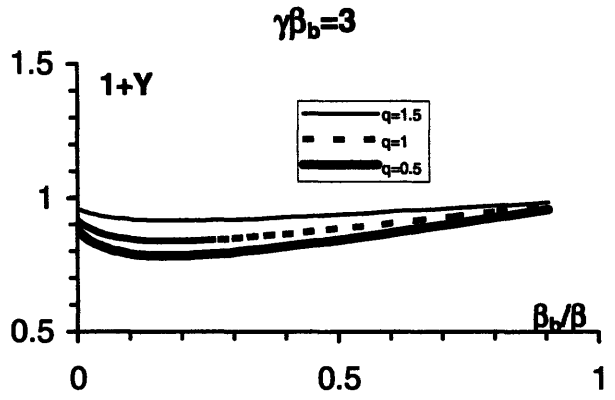

Figures 2.3: Graph of 1+Y vs. β_b/β for different values of q_h.

To determine the effects of a resonant hot electron population on the stability, we note that due to Eq. (2.53), the hot number density is monotonically decreasing, $rn'_{0h}/n_{0h} < 0$. Since $d < \gamma$ the stability is determined by the sign of Δ and therefore this hard core Z-pinch will remain stable for $\beta_h \sim \beta_b$ or $\beta_h >> \beta_b$ if $\eta_h > 2/3$ or $q_h > 4/5$.

Finally, we remark that if the unperturbed hot electron distribution function is simply assumed to be a drifting Maxwellian, then from Eq. (2.19) we find the flow $\vec{\mathbf{v}}_h = \hat{\mathbf{z}}(T_h n'_{0h}/m\Omega_e n_{0h})$ along with the restriction that $\nabla T_h = 0 = \eta_h$. As a result, for this "rigid rotor" equilibrium case, a weak resonant hot electron driven instability always occurs.

2.6. Hot Electron Interchange Mode

As another application of the preceding theory, we would like to briefly discuss another type of instability that is of interest to LDX and other closed field line devices. It is called the hot electron interchange mode[12,15] (HEI) for which the wave frequency is comparable to the

magnetic and/or diamagnetic hot particle frequency: $\langle\omega_{dh}\rangle \sim \omega >> \langle\omega_{de}\rangle$. In this limit the wave frequency dependencies of G, H, and I terms can no longer be ignored. Consequently, the dispersion relation given by Eq. (2.31) is no longer a simple quadratic and its solution has to be found numerically. In this section we present some sample numerical calculations and briefly mention the complications of obtaining stability conditions for the HEI.

For this frequency ordering the full expressions for G, H, and I are required, and can be written as

$$G = 1 - \frac{2}{\sqrt{\pi}} \int_0^\infty e^{-t^2} \frac{\omega - \omega_{*h}\left[1+\eta_h\left(t^2-\frac{3}{2}\right)\right]}{\omega_{kh}} \int_{-1}^{1} \frac{d\lambda}{\omega/\omega_{kh}t^2 - D} dt,$$

$$H = \frac{2}{\sqrt{\pi}} \int_0^\infty t^2 e^{-t^2} \frac{\omega - \omega_{*h}\left[1+\eta_h\left(t^2-\frac{3}{2}\right)\right]}{\omega_{kh}} \int_{-1}^{1} \frac{\left(1-\lambda^2\right)d\lambda}{\omega/\omega_{kh}t^2 - D} dt,$$

$$s_h I = \frac{\beta_h}{\sqrt{\pi}} \int_0^\infty t^4 e^{-t^2} \frac{\omega - \omega_{*h}\left[1+\eta_h\left(t^2-\frac{3}{2}\right)\right]}{\omega_{kh}} \int_{-1}^{1} \frac{\left(1-\lambda^2\right)^2 d\lambda}{\omega/\omega_{kh}t^2 - D} dt.$$

We substitute the preceding equations into the dispersion relation, Eq. (2.31) and numerically solve for ω. We present our findings in Figs. 2.4 in the form of graphs of $\mathrm{Re}(\omega)$ and $\mathrm{Im}(\omega)$ as a function of $n_{0h}T_e / p_{0b}$, which measures the fraction of hot electrons.

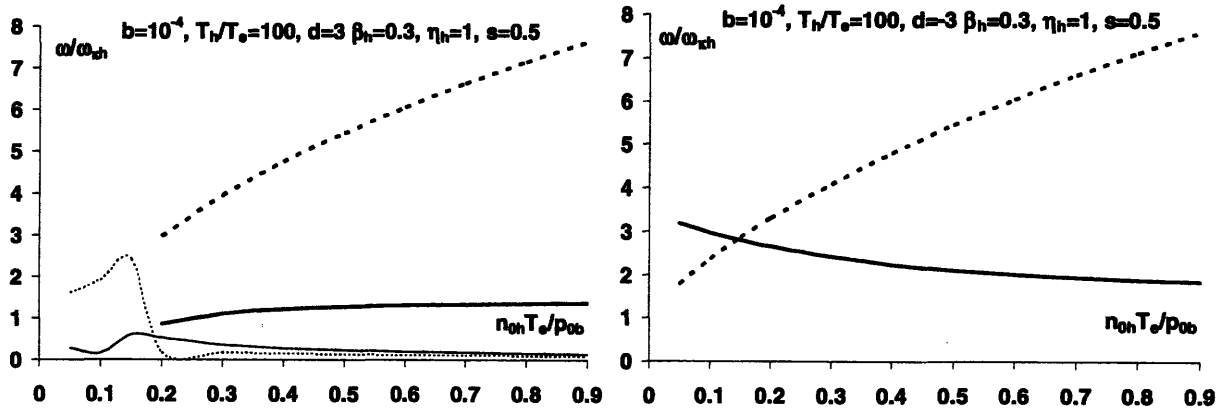

(a) (b)

Figures 2.4 (a)-(b): Real and imaginary parts of ω as a function of hot electron fraction, $n_{0h}T_e/p_{0b}$. The bold solid and dashed lines are real and imaginary parts for HEI mode, respectively. The fine solid and dashed lines are real and imaginary parts for MHD interchange mode, respectively.

Figure 2.4 (a) shows the usual MHD interchange instability in the presence of hot electrons; what we call the zero order instability. As $n_{0h}Te/p_{0b}$ increases we see that the region described by this parameter set is also unstable to the HEI mode. The graph suggests that these two modes might be coupled at $n_{0h}T_e/p_{0b}$ in the vicinity of 15%. Figure 2.4 (b) shows the case where the MHD mode is stable, while the HEI mode is unstable. This finding suggests that it is important to investigate not only the stability of the MHD mode, but also the HEI, as regions stable to the MHD mode can be unstable to the HEI. For the case shown in Fig. 2.4 (b) there also exists a stable root, which complicates the investigation of the stability of this mode in general. These results are merely intended to demonstrate another possible application of the theory developed, and are in no way intended to be exhaustive. Clearly much more work is required to find all possible branches of HEI mode and investigate the requirements for their stability.

2.7. Conclusions

The effects of hot electrons on the interchange stability of a Z-pinch plasma are investigated. The results yield two types of different resonant hot electron effects that modify the usual ideal MHD interchange stability condition.

Our analysis indicates that when the magnetic field is an increasing function of radius, there is a critical pitch angle for which the magnetic drift of hot electrons reverses direction. The interaction of the wave and the particles with the pitch angles close to critical always causes instability for Maxwellian hot electrons. Thus, stable operation is not possible when the magnetic field increases with radius.

If drift reversal ($s < 1$) does not occur and resonant hot electron effects are neglected, we find that interchange stability remains robust and is enhanced by increasing the background plasma pressure as well as the gradient of the hot electron density for $\beta_h >> \beta_b \sim 1$ case. However, once β_b becomes of order two or three, further increases in β_b do not result in significant increases in stability. In the absence of drift reversal, hot electron effects are weak, but not negligible. When they are retained, an additional constraint must be satisfied to avoid a weak resonant hot electron instability. For $\beta_h \sim \beta_b \sim 1$ and for $\beta_h >> \beta_b \sim 1$, the hot electron density and temperature profiles must satisfy $rn'_{0h} / n_{0h} > 3rT'_h / 2T_h$. Stability in the electrostatic limit ($\beta_b = 0$) is particularly awkward since it requires $rn'_{0h} / n_{0h} > 3rT'_h / 2T_h$ if there is no peak in the hot electron pressure profile.

Chapter 3

Effects of hot electrons on the stability of a dipolar plasma

3.1. Introduction

In Chapter 2 the effects of hot electrons on the interchange stability of Z-pinch plasma was investigated. In this section we extend our calculation to dipolar geometry for which the unperturbed magnetic field B_0 is purely in the poloidal direction, while the unperturbed diamagnetic current J_0 is toroidal. The format of this calculation is similar to that of the previous chapter, as we only consider flute or interchange modes with wave frequencies intermediate between the background and hot species drift frequencies, since they are the least stable modes in the absence of hot electrons[3-6]. We treat the magnetic drift, consisting of comparable grad B_0 and curvature drifts, on equal footing with the diamagnetic drift. We obtain the dispersion relation for arbitrary plasma and hot electron pressure, but then examine three plasma pressure orderings relative to the magnetic pressure: background electrostatic with $\beta_b << \beta_h \sim 1$, electromagnetic with $1 \sim \beta_b << \beta_h$, and electromagnetic with $1 \sim \beta_b \sim \beta_h$. Throughout this chapter we compare and contrast the results from dipolar geometry to that of the Z-pinch.

In Sec. 3.2 we derive two coupled equations for the ideal MHD background plasma that involve the perturbed hot electron number density and the $\nabla\psi$ component of the current. These two quantities are then evaluated kinetically in Sec. 3.3. Section 3.4 combines the results from the two previous sections to obtain the full dispersion relation, and general stability conditions,

including a discussion of hot electron drift resonance de-stabilization effects. As an application of the above theory, a separable form of a point dipole equilibrium is considered and the obtained results are presented in Sec. 3.5. We close with a brief discussion of the analysis in Sec. 3.6.

3.2. Ideal MHD Treatment of the Background Plasma

Our derivation for the dipole geometry will follow the guidelines developed for the Z-pinch. In this section we will use an ideal MHD treatment to derive the $\nabla\psi$ component of the perturbed Ampere's law and a perturbed quasi-neutrality condition. The quantities pertaining to the hot species, such as $\nabla\psi$ component of the perturbed current and number density, will be evaluated kinetically in the next section.

Using the standard approach for the closed field line axisymmetric or dipole configuration we introduce poloidal magnetic flux ψ, toroidal angle ζ and radial distance from the axis of symmetry R so that the unperturbed poloidal magnetic field and toroidal current are given by:

$$\vec{\mathbf{B}}_0 = \nabla\psi \times \nabla\zeta \text{ and } \vec{\mathbf{J}}_0 = R^2 \frac{dp_0}{d\psi} \nabla\zeta \tag{3.1}$$

where the total pressure p_0, is the sum of the hot pressure p_{0h} and the background pressure $p_{0b} = n_{0e}T_e + n_{0i}T_i$, with n_{0e}, n_{0i}, T_e, and T_i the background electron and ion densities and temperatures, respectively. The total current is the sum of the background and hot contributions $J_0 = J_{0b} + J_{0h}$ which separately satisfy the force balance relations to give

$\vec{\mathbf{J}}_{0b} = (dp_{0b}/d\psi)R^2\nabla\zeta$ and $\vec{\mathbf{J}}_{0h} = (dp_{0h}/d\psi)R^2\nabla\zeta$. Using the Ampere's law to derive the Grad-Shafranov equation yields

$$\nabla\cdot\left(\frac{\nabla\psi}{R^2}\right)+\mu_0\frac{dp_0}{d\psi}=0.$$

Defining $\vec{\kappa}=(\hat{\mathbf{b}}\cdot\nabla)\hat{\mathbf{b}}$ as magnetic field curvature with $\hat{\mathbf{b}}=\vec{\mathbf{B}}_0/B_0$, it also follows from the preceding equation and equilibrium pressure balance that

$$\frac{2\vec{\kappa}\cdot\nabla\psi}{B_0^2R^2}=\frac{\beta_0}{2}\frac{d\ln p_0}{d\psi}-\nabla\cdot\left(\frac{\nabla\psi}{B_0^2R^2}\right), \tag{3.2}$$

where

$$\beta_0\equiv\frac{2\mu_0 p_0}{B_0^2}.$$

We assume perturbations of the form $\hat{\mathbf{Q}}_1(\psi,\theta)e^{-i\omega t-il\zeta}$, with θ the poloidal angle and $\mathrm{Im}\,\omega>0$ for instability. Then, we perturb around this equilibrium by introducing the displacement vector $\vec{\xi}$ as $\vec{\mathbf{v}}_1=-i\omega\vec{\xi}$, with $\vec{\mathbf{v}}_1$ the background ion flow velocity, and writing it as

$$\vec{\xi}=\xi_B\frac{\vec{\mathbf{B}}_0}{B_0^2}+\xi_\psi\frac{\nabla\psi}{|\nabla\psi|^2}+\xi_\zeta\frac{\nabla\zeta}{|\nabla\zeta|^2}. \tag{3.3}$$

Using the usual ideal MHD equations, the perturbed electric field $\vec{\mathbf{E}}_1$, magnetic field $\vec{\mathbf{B}}_1$ and total current $\vec{\mathbf{J}}_1=\vec{\mathbf{J}}_{1b}+\vec{\mathbf{J}}_{1h}$ are given by

$$\vec{\mathbf{E}}_1=i\omega\vec{\xi}\times\vec{\mathbf{B}}_0, \tag{3.4}$$

$$\vec{\mathbf{B}}_1=\nabla\times\left(\vec{\xi}\times\vec{\mathbf{B}}_0\right), \text{ and} \tag{3.5}$$

$$\mu_0\vec{\mathbf{J}}_1=\nabla\times\vec{\mathbf{B}}_1, \tag{3.6}$$

where it is convenient to write $\vec{\mathbf{B}}_1$ as

$$\vec{\mathbf{B}}_1 = Q_B \frac{\vec{\mathbf{B}}_0}{B_0^2} + Q_\psi \frac{\nabla\psi}{|\nabla\psi|^2} + Q_\zeta \frac{\nabla\zeta}{|\nabla\zeta|^2}. \tag{3.7}$$

Equations (3.3) and (3.5) give $Q_B = -B_0^2\left(\frac{\nabla\zeta\cdot\nabla\xi_\zeta}{|\nabla\zeta|^2} + \frac{\nabla\psi\cdot\nabla\xi_\psi}{|\nabla\psi|^2}\right)$, $Q_\psi = \vec{\mathbf{B}}_0\cdot\nabla\xi_\psi$ and $Q_\zeta = \vec{\mathbf{B}}_0\cdot\nabla\xi_\zeta$.

In addition, background plasma momentum and energy conservation are written as

$$-m_i n_{0i}\omega^2\vec{\xi} = en_{0h}\vec{\mathbf{E}}_1 + \vec{\mathbf{J}}_{1b}\times\vec{\mathbf{B}}_0 + \vec{\mathbf{J}}_{0b}\times\vec{\mathbf{B}}_1 - \nabla p_{1b}, \tag{3.8}$$

and

$$p_{1b} = -\gamma p_{0b}\nabla\cdot\vec{\xi} - \frac{dp_{0b}}{d\psi}\xi_\psi, \tag{3.9}$$

where m_i denotes the mass of the background ions, p_{1b} is perturbed background pressure, and $\gamma = 5/3$. The $\vec{\mathbf{E}}_1$ term in the momentum equation, which is absent in the usual ideal MHD treatment, enters due to the effect of charge uncovering – the incomplete shielding of the background electrons by the background ions since the equilibrium quasineutrality for singly charged ions requires $n_{0h} = n_{0i} - n_{0e}$.

Using the preceding system of equations, it is convenient to define

$$W = -p_{1b} - \xi_\psi\frac{dp_{0b}}{d\psi} = \gamma p_{0b}\nabla\cdot\vec{\xi}, \tag{3.10}$$

and then obtain two coupled equations for W and ξ_ψ, both of which only require knowledge of the perturbed hot electron density and current, which are evaluated in the next section. To simplify the procedure we use the parallel component of Faraday's law and Eq. (3.3) to form $\nabla\cdot\vec{\xi}$ and to obtain two convenient expressions for ξ_ζ and Q_B

$$il\xi_\zeta = \frac{\nabla\psi\cdot\nabla\xi_\psi}{|\nabla\psi|^2} + \frac{Q_B}{B_0^2}, \tag{3.11}$$

and

$$\frac{Q_B}{B_0^2} = \vec{\mathbf{B}}_0 \cdot \nabla\left(\frac{\xi_B}{B_0^2}\right) + \xi_\psi \nabla \cdot \left(\frac{\nabla\psi}{|\nabla\psi|^2}\right) - \frac{W}{\gamma p_{0b}}. \tag{3.12}$$

Next, we consider the $\nabla\psi$ component of Ampere's law,

$$\mu_0 \vec{\mathbf{J}}_1 \cdot \nabla\psi = \mu_0 \vec{\mathbf{J}}_{1b} \cdot \nabla\psi + \mu_0 \vec{\mathbf{J}}_{1h} \cdot \nabla\psi = -ilQ_B - \vec{\mathbf{B}}_0 \cdot \nabla\left(R^2 Q_\zeta\right). \tag{3.13}$$

The background contribution is calculated from the toroidal component of the momentum equation yielding

$$\vec{\mathbf{J}}_{1b} \cdot \nabla\psi = m_i n_{0i} \omega^2 R^2 \xi_\zeta + e n_{0h} R^2 \vec{\mathbf{E}}_1 \cdot \nabla\zeta + ilp_{1b},$$

with ξ_ζ given by Eq. (3.11), p_{1b} given by Eq. (3.10), and $\vec{\mathbf{E}}_1 \cdot \nabla\zeta = -i\omega|\nabla\zeta|^2 \xi_\psi$ from the toroidal component of Eq. (3.4). Defining the background plasma beta as

$$\beta_b \equiv \frac{2\mu_0 p_{0b}}{B_0^2},$$

and using Eq. (3.11), the $\nabla\psi$ component of Ampere's law can be rewritten as

$$\begin{aligned} &-\frac{\mu_0 \vec{\mathbf{J}}_{1h} \cdot \nabla\psi}{ilB_0^2} - \frac{\vec{\mathbf{B}}_0 \cdot \nabla\left(R^2 Q_\zeta\right)}{ilB_0^2} + \frac{\beta_b W}{2p_{0b}} + \frac{1}{2}\beta_b \left(\frac{d\ln p_{0b}}{d\psi}\xi_\psi + \frac{\omega e n_{0h}}{l p_{0b}}\xi_\psi + \frac{m_i n_{0i}\omega^2 R^2}{l^2 p_{0b}} \frac{\nabla\psi \cdot \nabla\xi_\psi}{|\nabla\psi|^2}\right) \\ &= \left(1 - \beta_b \frac{m_i n_{0i}\omega^2 R^2}{2l^2 p_{0b}}\right)\frac{Q_B}{B_0^2}. \end{aligned} \tag{3.14}$$

The most unstable ideal MHD ballooning-interchange modes have $l >> 1$ for an axisymmetric torus with closed field lines[3]. Therefore, we can use the standard high mode number formalism to neglect the $1/l^2$ term from $\vec{\mathbf{B}}_0 \cdot \nabla\left(R^2 Q_\zeta\right)$ and the coupling to the magnetosonic waves by assuming $\omega^2 R^2 / l^2 << p_{0b} / m_i n_{0i}$ in Eq. (3.14). Then, using Eq. (3.12) we obtain the first of the desired equations, the $\nabla\psi$ component of Ampere's law, in the form:

$$\frac{W}{\gamma p_{0b}}\left(1+\frac{1}{2}\gamma\beta_b\right)=\vec{\mathbf{B}}_0\cdot\nabla\left(\frac{\xi_B}{B_0^2}\right)+\left[\nabla\cdot\left(\frac{\nabla\psi}{|\nabla\psi|^2}\right)-\frac{\beta_b}{2}\left(\frac{d\ln p_{0b}}{d\psi}+\frac{\omega\varepsilon n_{0h}}{lp_{0b}}\right)\right]\xi_\psi+\frac{\mu_0\vec{\mathbf{J}}_{1h}\cdot\nabla\psi}{ilB_0^2}. \qquad (3.15)$$

To obtain the second equation, we start with background charge conservation in the form $\nabla\cdot\vec{\mathbf{J}}_{1b}=i\omega e(n_{1i}-n_{1e})=i\omega\varepsilon n_{1h}$, where we also use perturbed quasi-neutrality. The expressions for the parallel and perpendicular components of the perturbed background current are calculated from the parallel component of Ampere's law and momentum equation, respectively. Using the large l approximation gives

$$\mu_0\vec{\mathbf{J}}_1\cdot\vec{\mathbf{B}}_0=\mu_0\left(\vec{\mathbf{J}}_{1b}+\vec{\mathbf{J}}_{1h}\right)\cdot\vec{\mathbf{B}}_0=\frac{1}{R^2}\nabla\psi\cdot\nabla\left(R^2Q_\zeta\right)+\frac{ilQ_\psi}{R^2}\approx+\frac{ilQ_\psi}{R^2},$$

$$\vec{\mathbf{J}}_{1b}\cdot\nabla\psi=-i\omega\varepsilon n_{0h}\xi_\psi+ilp_{1b}+m_in_{0i}\omega^2R^2\xi_\zeta\approx-i\omega\varepsilon n_{0h}\xi_\psi+ilp_{1b},$$

and

$$\vec{\mathbf{J}}_{1b}\cdot\nabla\zeta=\frac{\nabla\psi\cdot\nabla p_{1b}}{|\nabla\psi|^2}-\frac{m_in_{0i}\omega^2}{|\nabla\psi|^2}\xi_\psi-\frac{e\varepsilon n_{0h}\omega}{l}\left(\frac{\nabla\psi\cdot\nabla\xi_\psi}{|\nabla\psi|^2}+\frac{Q_B}{B_0^2}\right)-\frac{dp_{0b}}{d\psi}\frac{Q_{B_0}}{B_0^2}.$$

Notice that we retain the inertial term in $\vec{\mathbf{J}}_{1b}\cdot\nabla\zeta$, but continue to ignore it in $\vec{\mathbf{J}}_{1b}\cdot\nabla\psi$ to be consistent with the large l expansion. Expressing p_{1b} and Q_{B_0} in terms of W and ξ_ψ, we insert the preceding three equations into the background charge conservation to obtain

$$\begin{aligned}\frac{\omega\varepsilon n_{1h}}{l}=&\vec{\mathbf{B}}_0\cdot\nabla\left(\frac{\vec{\mathbf{B}}_0\cdot\nabla\xi_\psi}{\mu_0|\nabla\psi|^2}-\frac{\vec{\mathbf{J}}_{1h}\cdot\vec{\mathbf{B}}_0}{ilB_0^2}\right)-\left[\nabla\cdot\left(\frac{\nabla\psi}{|\nabla\psi|^2}\right)+\frac{1}{\gamma}\frac{d\ln p_{0b}}{d\psi}+\frac{\omega\varepsilon n_{0h}}{l\gamma p_{0b}}\right]W\\&+\left(\frac{m_in_{0i}\omega^2}{R^2B_0^2}-\frac{\omega\varepsilon\nabla\psi\cdot\nabla n_{0h}}{lR^2B_0^2}\right)\xi_\psi+\left(\frac{dp_{0b}}{d\psi}+\frac{\omega\varepsilon n_{0h}}{l}\right)\vec{\mathbf{B}}_0\cdot\nabla\left(\frac{\xi_B}{B_0^2}\right).\end{aligned} \qquad (3.16)$$

Finally, using the parallel component of the momentum equation to eliminate ξ_B yields

$$\vec{\mathbf{B}}_0\cdot\nabla\left(\frac{\xi_B}{B_0^2}\right)=-\vec{\mathbf{B}}_0\cdot\nabla\left(\frac{\vec{\mathbf{B}}_0\cdot\nabla W}{m_in_{0i}\omega^2B_0^2}\right), \qquad (3.17)$$

where we assume n_{0i} is a flux function. Substituting Eq. (3.17) into Eqs. (3.15) and (3.16) we now have the two coupled equations

$$-\frac{\mu_0 \vec{J}_{1h}\cdot\nabla\psi}{ilB_0^2}+\vec{B}_0\cdot\nabla\left(\frac{\vec{B}_0\cdot\nabla W}{m_i n_{0i}\omega^2 B_0^2}\right)=-\frac{W}{\gamma p_{0b}}\left(1+\frac{1}{2}\gamma\beta_b\right)+\left[\nabla\cdot\left(\frac{\nabla\psi}{|\nabla\psi|^2}\right)-\frac{\beta_b}{2}\left(\frac{d\ln p_{0b}}{d\psi}+\frac{\omega\varepsilon n_{0h}}{lp_{0b}}\right)\right]\xi_\psi \tag{3.18}$$

and

$$\frac{n_{1h}T_e}{p_{0b}}+\left(-\frac{lT_e}{\omega\varepsilon p_{0b}}\frac{m_i n_{0i}\omega^2}{B_0^2R^2}+\frac{n_{0h}T_e}{p_{0b}}\frac{\nabla\psi\cdot\nabla\ln n_{0h}}{|\nabla\psi|^2}\right)\xi_\psi=-\frac{W}{\gamma p_{0b}}\left\{\frac{lT_e}{\omega\varepsilon}\left[\frac{d\ln p_{0b}}{d\psi}+\gamma\nabla\cdot\left(\frac{\nabla\psi}{|\nabla\psi|^2}\right)\right]+\frac{n_{0h}T_e}{p_{0b}}\right\}+$$
$$-\left(\frac{lT_e}{\omega\varepsilon}\frac{d\ln p_{0b}}{d\psi}+\frac{n_{0h}T_e}{p_{0b}}\right)\vec{B}_0\cdot\nabla\left(\frac{\vec{B}_0\cdot\nabla W}{m_i n_{0i}\omega^2 B_0^2}\right)+\frac{lT_e}{\omega\varepsilon p_{0b}}\vec{B}_0\cdot\nabla\left(\frac{\vec{B}_0\cdot\nabla\xi_\psi}{\mu_0|\nabla\psi|^2}-\frac{\vec{J}_{1h}\cdot\vec{B}_0}{ilB_0^2}\right), \tag{3.19}$$

where the terms with n_{0h} are due to the charge uncovering effect of the hot electrons on quasi-neutrality.

Observe that without hot electrons we can easily recover the well known ballooning equation for shear Alfven modes[3]. It can be obtained by substituting Eq. (3.18) and its poloidal flux surface average into Eq. (3.19) to first eliminate $\vec{B}_0\cdot\nabla W$ and then the W terms, respectively:

$$B_0^2R^2\vec{B}_0\cdot\nabla\left(\frac{\vec{B}_0\cdot\nabla\xi_\psi}{\mu_0|\nabla\psi|^2}\right)+\xi_\psi\left(2\vec{\kappa}\cdot\nabla p_{0b}+m_i n_{0i}\omega^2\right)=4\gamma p_{0b}\left(\vec{\kappa}\cdot\nabla\psi\right)\frac{\left\langle\xi_\psi\vec{\kappa}\cdot\nabla\psi/B_0^2R^2\right\rangle}{\left(1+\frac{1}{2}\gamma\langle\beta_b\rangle\right)}.$$

In addition to using Eq. (3.2) to get the right hand side of the preceding equation, we note that it follows from Eq. (3.18) that the variations of W along the unperturbed magnetic field are proportional to ω^2. As a result, W tends to flux function as the growth rate diminishes. In particular, from the field line average of Eq. (3.18)

$$W \approx -2\gamma p_{0b} \frac{\left\langle \xi_\psi \vec{\kappa} \cdot \nabla \psi / B_0^2 R^2 \right\rangle}{\left(1+\frac{1}{2}\gamma \langle \beta_b \rangle\right)},$$

where the flux surface average is defined by $\langle \ldots \rangle = V^{-1} \oint (\ldots) d\theta / \vec{\mathbf{B}}_0 \cdot \nabla \theta$ with θ the poloidal angle and $V = \oint d\theta / \vec{\mathbf{B}}_0 \cdot \nabla \theta$.

3.3 Kinetic Treatment Of The Hot Electrons

In the previous section we have obtained two coupled equations for quasineutrality and Ampere's law that require knowledge of the perturbed hot electron density and current. Generalizing the Z-pinch procedure developed in reference[16] to dipole geometry, we will first kinetically evaluate the perturbed hot electron responses in this section to obtain the dispersion relation in the next section. We assume that the temperature of the hot electron population, T_h, is much larger that the background temperatures, which requires that the magnetic drift and diamagnetic frequencies of the hot electrons to be much larger than the corresponding background frequencies.

We assume that the hot electrons satisfy the Vlasov equation, and following the standard procedure for solving the gyro-kinetic equation[9,10] we linearize the hot electron distribution function around the equilibrium by writing $f_h = f_{0h} + f_{1h} + \ldots$. Employing the orderings

$$\Omega_e \geq \omega_b >> \omega_{dh} \sim \omega_{*h} >> \omega, \tag{3.20}$$

with m the electron mass, $\Omega_e = eB_0/m$ the cyclotron frequency, $\omega_b \sim \vec{\mathbf{v}}_\parallel \cdot \nabla$ the bounce frequency, and ω_{dh} and ω_{*h} the magnetic and diamagnetic frequencies, the equilibrium distribution function satisfies

$$\vec{\mathrm{v}}\cdot\nabla f_{0h}-\Omega_e\vec{\mathrm{v}}\times\hat{\mathbf{b}}\cdot\nabla_{\mathrm{v}}f_{0h}=\vec{\mathrm{v}}\cdot\nabla f_{0h}+\Omega_e\frac{\partial f_{0h}}{\partial\phi}=0, \tag{3.21}$$

where ϕ is gyrophase. As in the case of all axisymmetric machines, the toroidal component of canonical angular momentum is a constant of the motion and therefore it is useful to introduce $\psi_*=\psi-\frac{mR}{e}\hat{\zeta}\cdot\vec{\mathrm{v}}$. Then exact solutions to Eq. (3.21) exist of the form $f_{0h}=f_{0h}(E,\psi_*)$, with $E=\mathrm{v}^2/2$.

To evaluate the first order correction to the hot electron distribution function we again look for solutions of the form $e^{-i\omega t-il\zeta}$ and solve the linearized Vlasov kinetic equation

$$\frac{\partial f_{1h}}{\partial t}+\vec{\mathrm{v}}\cdot\nabla f_{1h}-\Omega_e\vec{\mathrm{v}}\times\hat{\mathbf{b}}\cdot\nabla_{\mathrm{v}}f_{1h}+\frac{e}{m}\left(\nabla\Phi+\frac{\partial\vec{\mathbf{A}}}{\partial t}-\vec{\mathrm{v}}\times\vec{\mathbf{B}}_1\right)\cdot\nabla_{\mathrm{v}}f_{0h}=0, \tag{3.22}$$

where the scalar and vector potentials Φ and $\vec{\mathbf{A}}=A_{\|}\hat{\mathbf{b}}+A_{\psi}\nabla\psi/RB_0+A_{\zeta}R\nabla\zeta$, enter $\vec{\mathbf{E}}_1=-\nabla\Phi-\partial\vec{\mathbf{A}}/\partial t$ and $\vec{\mathbf{B}}_1=\nabla\times\vec{\mathbf{A}}$, with $\nabla\cdot\vec{\mathbf{A}}=0$ for the Coulomb gauge. Observe that the gauge condition coupled with the large mode number assumption causes the toroidal component of the vector potential to be small compared with the other two components: $A_{\zeta}\sim(A_{\psi}\ or\ A_{\|})/l$.

The solution to Eq. (3.22) is found by removing the adiabatic piece by writing

$$f_{1h}=\frac{e\Phi}{T_h}f_{0h}+g_1, \tag{3.23}$$

and then defining $g_1=\bar{g}_1+\tilde{g}_1$ with the bar and tildes indicating the gyrophase independent and dependent parts, respectively. Using v, magnetic moment $\mu=\mathrm{v}_{\perp}^2/2B_0$, ϕ as the velocity space variables, and the incremental time along the particles trajectory $d\tau\equiv\frac{d\theta}{\vec{\mathrm{v}}_{\|}\cdot\nabla\theta}>0$, the resulting lowest order expressions for $\bar{g}_1$ and $\tilde{g}_1$ are given by[12,13]

$$\bar{g}_1=-\frac{f_{Mh}\left(\omega-\omega_h^T\right)}{\left(\omega-\frac{m\mathrm{v}^2}{2T_h}\omega_D\right)}\left(\frac{e}{T_h}\frac{\oint d\tau\left(\Phi-\mathrm{v}_{\|}A_{\|}\right)}{\oint d\tau}-\frac{m\mu}{T_h}\frac{\oint d\tau Q_B/B_0}{\oint d\tau}\right) \tag{3.24}$$

and

$$\tilde{g}_1 = -\Omega_e^{-1}\tilde{\mathbf{v}}_\perp \times \hat{\mathbf{b}} \cdot \left[\nabla \bar{g}_1 + \frac{ie\omega}{T_h} f_{Mh} \tilde{\mathbf{A}} - \frac{Q_B}{B_0^2} \frac{\partial f_{Mh}}{\partial \psi} \nabla \psi \right], \tag{3.25}$$

where the parallel and perpendicular subscripts refer to the components parallel and perpendicular to the equilibrium magnetic field $\vec{\mathbf{B}}_0$. The details of the calculation are given in the Appendix 3.A. For simplicity we consider the unperturbed hot electron distribution function f_{0h} to be a Maxwellian to the lowest order and use a gyroradius expansion to write $f_{0h}(E,\psi_*) = f_{Mh} + (\psi_* - \psi)\partial f_{Mh}/\partial\psi + \ldots$ with $f_{Mh} = n_{0h}(m/2\pi T_h)^{3/2}\exp\left(-m\mathrm{v}^2/2T_h\right)$. The hot electron diamagnetic drift frequency is defined by

$$\omega_{*h}^T = \omega_{*h}\left[1 + \eta_h\left(\frac{m\mathrm{v}^2}{2T_h} - \frac{3}{2}\right)\right], \tag{3.26}$$

with $\omega_{*h} = \frac{lT_h}{e}\frac{d\ln n_{0h}}{d\psi}$ and $\eta_h = d\ln T_h / d\ln n_{0h}$. The effective trajectory averaged magnetic drift frequency is

$$\omega_D = \oint \frac{2lT_h \vec{\kappa}\cdot\nabla\psi}{eR^2B_0^2}\left[1 - \frac{B_0(1+s)}{2\bar{B}}\lambda\right]d\tau / \oint d\tau = -\frac{2lT_h}{m\mathrm{v}^2}\oint \vec{\mathbf{v}}_d \cdot \nabla\zeta d\tau / \oint d\tau, \tag{3.27}$$

with

$$\vec{\mathbf{v}}_d \cdot \nabla\zeta = -\frac{\mathrm{v}^2\vec{\kappa}\cdot\nabla\psi}{\Omega_e R^2 B_0}\left[1 - \frac{B_0(1+s)}{2\bar{B}}\lambda\right], \tag{3.28}$$

where

$$s = 1 - \frac{\nabla\psi\cdot\nabla\ln B_0}{\vec{\kappa}\cdot\nabla\psi} \tag{3.29}$$

measures the departure from the vacuum limit $s = 0$ and $\lambda = \frac{\mathrm{v}_\perp^2}{\mathrm{v}^2}\frac{\bar{B}}{B_0} = \frac{\mu\bar{B}}{E}$ is a pitch angle variable with $\bar{B}$ being the value of B_0 at the outboard equatorial plane. We note that the trajectory

integrals are different for passing and trapped particles, with the former running over one full poloidal pass, while the latter runs over one complete bounce.

Ampere's law, Eq. (3.18), and, quasi-neutrality Eq. (3.19), require the hot electron density and $\nabla\psi$ component of perturbed hot electron current, which we form by integrating the distribution function over velocity space to obtain $n_{1h} = \int f_{1h} d\bar{\mathbf{v}}$ and $J_{1\psi} = -e\int \mathrm{v}_\psi f_{1h} d\bar{\mathbf{v}}$. Only the gyrophase independent part of g_1 contributes to n_{1h}, while only the gyrophase dependent part survives the integration in $J_{1\psi}$. The full details of the preceding calculations are presented in Appendix 3.B.

From the form of f_1 it is clear that both n_{1h} and $J_{1\psi}$ involve $d\tau$ integrals, which involve poloidal trajectory averages of Φ, $A_\parallel$, and Q_B. In Z-pinch geometry[16] the interchange assumption removed poloidal variations. As a result, the perturbed number density and radial component of current were written as linear combinations of Φ and Q_B, while the parallel component of the Ampere's law resulted in a homogeneous equation for $A_\parallel$, allowing us to set it to zero. These simplifications permitted us to write quasineutrality and the radial component of Ampere's law as a set of two linearly coupled equations. In dipole geometry, the poloidal variation of B_0 and $\vec{\kappa}$ cause quasineutrality and the $\nabla\psi$ component of Ampere's law to become a set of two coupled integro-differential equations, which without approximations can only be solved numerically.

To examine the possibility of a partially analytic solution we consider interchange modes, with $Q_\psi = \vec{\mathbf{B}}_0 \cdot \nabla\xi_\psi = 0$, making ξ_ψ a flux function. Next, we examine $\nabla\psi$ and $\nabla\zeta$ components of Ohm's law, Eq. (3.4),

$$\vec{\mathbf{E}}_1 \cdot \nabla \psi = -\nabla \Phi \cdot \nabla \psi + i\omega A_\psi R B_0 = i\omega \xi_\zeta R^2 B_0^2$$
$$\vec{\mathbf{E}}_1 \cdot \nabla \zeta = il\Phi / R^2 + i\omega A_\zeta / R = -i\omega \xi_\psi / R^2.$$

We recall that from Eq. (3.11) $\xi_\zeta \sim \xi_\psi / R^2 B_0 l$, while from $\nabla \cdot \vec{\mathbf{A}} = 0$ we have $A_\zeta \sim A_\psi / l$. As a result, in the preceding expression for $\vec{\mathbf{E}}_1 \cdot \nabla \zeta$ we may neglect the A_ζ term as small by $1/l^2$, making

$$\Phi = -\omega \xi_\psi / l \tag{3.30}$$

We also note that

$$A_\psi \sim \xi_\psi / lR. \tag{3.31}$$

For interchange modes Φ is up-down symmetric, while $A_\parallel$ is antisymmetric. As a result, for both the passing and trapped particles $\oint v_\parallel A_\parallel d\tau = 0$ and $\vec{\mathbf{J}}_{1h} \cdot \vec{\mathbf{B}}_0 \propto \oint v_\parallel \bar{g}_1 d\vec{\mathbf{v}} = 0$. Consequently, we may ignore $\vec{\mathbf{J}}_{1h} \cdot \vec{\mathbf{B}}_0$ and $A_\parallel$ terms in Eqs. (3.18), (3.19), and (3.24). In addition, upon gyroaveraging, the Q_B term in Eq. (3.25) does not survive to enter $\vec{\mathbf{J}}_{1h} \cdot \nabla \psi$ and the A_ζ component that does enter is small by $1/l^2$ as shown in Appendix 3.B.

The last complication in Eqs. (3.24) and (3.25) is the trajectory averaged terms involving Q_B. If we combine Eqs. (3.12), (3.17) and (3.18) to eliminate terms involving $\vec{\mathbf{B}}_0 \cdot \nabla$ we get

$$\frac{Q_B}{\mu_0} = -\frac{\vec{\mathbf{J}}_{1h} \cdot \nabla \psi}{il} + W + \left(\frac{dp_{0b}}{d\psi} + \frac{\omega e n_{0h}}{l} \right) \xi_\psi . \tag{3.32}$$

For ideal MHD interchange modes near marginality both ξ_ψ and W are flux functions, so we see from Eq. (3.32) that in the absence of hot electrons, Q_B is also a flux function. Therefore, near marginality any variations of Q_B along the equilibrium magnetic field are caused by $\nabla \psi$ component of the hot electron current. In general $\vec{\mathbf{J}}_{1h} \cdot \nabla \psi$ and, as a result, Q_B, W, and ξ_ψ are

not flux functions, causing the quasineutrality and $\nabla\psi$ component of Ampere's law to be coupled integro-differential equations. There are several options to deal with the increased complexity. One is to solve the problem numerically, which is outside the scope of the present work and probably not the most insightful approach at this point in the development of hot electron models. The second option is to treat perturbed hot electron terms as small and introduce them perturbatively. However, from the Z-pinch geometry, we know that hot electron effects can enter on equal footing with the fluid background response and play an important role in stability analysis. The third option, and the one we will pursue here, is to simply assume that Q_B, W, Φ, and $\vec{\mathbf{J}}_{1h}\cdot\nabla\psi$ are flux functions to lowest order, which allows us to obtain a dispersion relation essentially the same as the one found for a Z-pinch[16]. This procedure allows us to recover all the results from the second option, but cannot otherwise be justified in any other rigorous fashion. However, when we consider the point dipole model in Sec. V, we will find that the behavior of I, H, F, and G as a function of poloidal angle is similar to that of B_0^{-2} as required for this assumption.

Replacing Q_B, $\vec{\mathbf{J}}_{1h}\cdot\nabla\psi$ and Φ by $\langle Q_B\rangle=\langle B_\parallel B_0\rangle$, $\langle\vec{\mathbf{J}}_{1h}\cdot\nabla\psi\rangle$, and $\langle\Phi\rangle$, and taking them outside of poloidal trajectory averages in Eq. (3.24). To lowest significant order, we can then write the expressions for n_{1h} and $\langle\vec{\mathbf{J}}_{1h}\cdot\nabla\psi\rangle$ as

$$\frac{n_{1h}}{n_{0h}}=\frac{e\langle\Phi\rangle}{T_h}G+\langle Q_B\rangle\langle B_0^{-2}\rangle H \tag{3.33}$$

and

$$\frac{\mu_0\langle\vec{\mathbf{J}}_{1h}\cdot\nabla\psi\rangle}{ilB_0^2}=-\frac{\langle\beta_h\rangle}{2}\left(\frac{e\langle\Phi\rangle}{T_h}F-\langle Q_B\rangle\langle B_0^{-2}\rangle I\right), \tag{3.34}$$

where $\beta_h=2\mu_0 p_{0h}/B_0^2$ and

$$G=1-\frac{1}{n_{0h}}\int d\vec{v}\frac{f_{Mh}\left(\omega-\omega_{*h}^{T}\right)}{\left(\omega-\frac{mv^2}{2T_h}\omega_D\right)},\ H=\frac{\left\langle B_0^{-2}\right\rangle^{-1}}{n_{0h}\bar{B}^2}\int d\vec{v}\frac{mv^2}{2T_h}\frac{\lambda f_{Mh}\left(\omega-\omega_{*h}^{T}\right)\oint d\tau(\bar{B}/B_0)/\oint d\tau}{\left(\omega-\frac{mv^2}{2T_h}\omega_D\right)},$$
$$F=\frac{\left\langle B_0^{-2}\right\rangle^{-1}}{n_{0h}B_0\bar{B}}\int d\vec{v}\frac{mv^2}{2T_h}\frac{\lambda f_{Mh}\left(\omega-\omega_{*h}^{T}\right)}{\left(\omega-\frac{mv^2}{2T_h}\omega_D\right)},\ I=\frac{\left\langle B_0^{-2}\right\rangle^{-2}}{n_{0h}B_0\bar{B}^3}\int d\vec{v}\left(\frac{mv^2}{2T_h}\right)^2\frac{\lambda^2 f_{Mh}\left(\omega-\omega_{*h}^{T}\right)\oint d\tau(\bar{B}/B_0)/\oint d\tau}{\left(\omega-\frac{mv^2}{2T_h}\omega_D\right)}. \tag{3.35}$$

The details of obtaining these expressions are provided in Appendix 3.B. Notice, that in general, the expressions for G, H, F, and I contain resonant particle effects due to the possible vanishing of the denominator. Here we consider only the intermediate frequency ordering, with the wave frequency much less than the magnetic frequency of the hot electrons, so that the ω dependence in the preceding equations only matters in determining the causal path of integration about the singularity. The vanishing of the denominator corresponds to the wave – hot electron drift resonance, which can occur when ω_D is small. This resonance is weak when only very low speed hot electrons interact with the wave (no drift reversal), and possible strong for $s>1$ when drift reversal occurs so that many hot electrons with a specific pitch angle $\lambda_{crit}=\frac{2\bar{B}}{B_0(1+s)}$ can resonate.

3.4 Dispersion Relation

In this section we obtain the dispersion relation by substituting the expressions for $\langle n_{1h}\rangle$ and $\left\langle \vec{\mathbf{J}}_{1h}\cdot\nabla\psi\right\rangle\left\langle B_0^{-2}\right\rangle$ given by Eqs. (3.33) and (3.34) into quasineuitrality and the $\nabla\psi$ component of Ampere's law. To annihilate terms involving $\vec{\mathbf{B}}_0\cdot\nabla$ in Eqs. (3.18) and (3.19) we flux surface average and then assume $\Phi=\langle\Phi\rangle$, $W=\langle W\rangle$, $Q_B=\langle Q_B\rangle$, and

$\vec{J}_{1h}\cdot\nabla\psi=\langle\vec{J}_{1h}\cdot\nabla\psi\rangle$ in undifferentiated terms, and continue to use $\oint v_{\parallel}A_{\parallel}d\tau=0=\vec{J}_{1h}\cdot\vec{B}_0$. When we use Eq. (3.12) to eliminate $\langle W\rangle$, the resulting two coupled equations are identical in form to those obtained for a Z-pinch[16]:

$$Q_B\langle B_0^{-2}\rangle\left(1+\tfrac{1}{2}\gamma\langle\beta_b\rangle\right)=-\frac{\mu_0}{il}\langle B_0^{-2}\rangle\langle\vec{J}_{1h}\cdot\nabla\psi\rangle+\frac{\langle\beta_b\rangle}{2}\left[\frac{\langle\omega_{de}\rangle}{\omega}(\gamma-d)-\frac{n_{0h}T_e}{p_{0b}}\right]\frac{e\Phi}{T_e} \tag{3.36}$$

and

$$\left\langle\frac{n_{1h}T_e}{p_{0b}}\right\rangle+\left[\langle b\rangle+\frac{\langle\omega_{de}\rangle}{\omega}\frac{n_{0h}T_e}{p_{0b}}\left(1+\frac{d\ln n_{0h}}{d\ln V}\right)-\frac{\langle\omega_{de}\rangle^2}{\omega^2}(\gamma-d)\right]\frac{e\Phi}{T_e}=Q_B\langle B_0^{-2}\rangle\left[\frac{n_{0h}T_e}{p_{0b}}-\frac{\langle\omega_{de}\rangle}{\omega}(\gamma-d)\right], \tag{3.37}$$

where we define

$$d=-\frac{d\ln p_{0b}}{d\ln V},\ \langle\omega_{de}\rangle=-\frac{lT_e}{e}\frac{d\ln V}{d\psi},\ b=\frac{l^2T_e}{e^2B_0^2R^2}\frac{m_in_{0i}T_e}{p_{0b}},$$

and employ $\left\langle\nabla\cdot\left(\nabla\psi/|\nabla\psi|^2\right)\right\rangle=d\ln V/d\psi$. Combining the preceding two equations with Eqs. (3.33) and (3.34) to form the dispersion relation we obtain

$$\begin{aligned}&\left[\langle b\rangle+\frac{n_{0h}T_e}{p_{0b}}\left[\frac{T_e}{T_h}\langle G\rangle+\frac{\langle\omega_{de}\rangle}{\omega}\left(1+\frac{d\ln n_{0h}}{d\ln V}\right)\right]-\frac{\langle\omega_{de}\rangle^2}{\omega^2}(\gamma-d)\right]\left(1+\tfrac{1}{2}\gamma\langle\beta_b\rangle+\frac{\langle\beta_h\rangle}{2}\langle I\rangle\right)+\\&+\frac{\langle\beta_b\rangle}{2}\left[\frac{\langle\omega_{de}\rangle}{\omega}(\gamma-d)-\frac{n_{0h}T_e}{p_{0b}}\left(1-\langle F\rangle\right)\right]\left[\frac{\langle\omega_{de}\rangle}{\omega}(\gamma-d)-\frac{n_{0h}T_e}{p_{0b}}\left(1-\langle H\rangle\right)\right]=0,\end{aligned} \tag{3.38}$$

which is the same as the Z-pinch result[16] with the exception of flux surface and trajectory averages due to geometrical effects.

Even though, the dispersion relation looks quadratic in ω, in general, the coefficients of the above dispersion relation are not necessarily real or independent of the wave frequency due to the hot electron drift resonance with the wave. As we noted in the previous section, there are two types of resonance. A weak resonance occurs when the wave interacts with a few slow moving hot electrons. In this case, even though the imaginary parts of the coefficients in the

above dispersion relation depend on the wave frequency, they are much smaller than the real parts. As a result, this type of resonance can be examined perturbatively, which is done later in the section. Another type of resonance happens when $s>1$ and drift reversal is possible. In this case the wave interacts the hot electrons of particular pitch angles, the real and imaginary parts of the coefficients are comparable in size, and the interaction is strong and always unstable. In the remainder of this section we discuss stability assuming drift reversal does not occur.

We will not consider the high frequency regime having $\langle\omega_{dh}\rangle \sim \omega >> \langle\omega_{de}\rangle$. We simply remark that in this limit the wave frequency dependencies of $\langle G\rangle$, $\langle H\rangle$, $\langle F\rangle$, and $\langle I\rangle$ terms can no longer be ignored. Consequently, the dispersion relation given by Eq. (3.38) is no longer a simple quadratic and its solution has to be found numerically. In this case, a new instability can occur which is often referred to as the hot electron interchange[11].

In what follows we first consider the lowest order interchange modes in the absence of resonant hot electrons for $\omega << \langle\omega_{dh}\rangle \sim \omega_{*h}$ and then retain the hot electron drift resonance perturbatively.

3.4.A. Lowest order non-resonant modes.

To investigate the effects of hot electrons on stability for closed magnetic field lines, we first ignore any resonant effects and consider the electrostatic case. To do so we drop all the terms proportional to the background plasma, by assuming $\beta_b << \beta_h \sim 1$. The dispersion relation then reduces to

$$\left(1+\frac{\langle\beta_h\rangle}{2}\langle I\rangle\right)\left[\frac{\omega^2}{\langle\omega_{de}\rangle^2}\langle b\rangle+\frac{n_{0h}T_e}{p_{0b}}\frac{\omega}{\langle\omega_{de}\rangle}\left(1+\frac{d\ln n_{0h}}{d\ln V}\right)-(\gamma-d)\right]=0. \qquad (3.39)$$

The overall multiplier in front is independent of the frequency, so stability requires $(n_{0h}T_e/p_{0b})^2\left(1+\frac{d\ln n_{0h}}{d\ln V}\right)^2+4\langle b\rangle(\gamma-d)\geq 0$, as in a Z-pinch[16]. The hot electrons enter only through charge uncovering effects (proportional to n_{0h}) in this limit and these improve the well known dipole interchange stability condition[3,5] of $d<\gamma$.

For the fully electromagnetic case, we continue to ignore the resonant effects of the hot electrons so that $\langle G\rangle$, $\langle H\rangle$, $\langle F\rangle$, and $\langle I\rangle$ are real and independent of wave frequency and the dispersion relation is quadratic. For the intermediate frequency ordering with $\langle\omega_{dh}\rangle >> \omega >> \langle\omega_{de}\rangle$ it follows that $\frac{T_h}{T_e}=\frac{\langle\omega_{dh}\rangle}{\langle\omega_{de}\rangle}>>\frac{\omega}{\langle\omega_{de}\rangle}$. It is expected that during LDX operation the hot electron beta will be much larger than the background beta so it is of interest to consider $\beta_h >> \beta_b \sim 1$, which coupled with the frequency ordering allows us to take $\frac{n_{0h}T_e}{p_{0b}}\sim\frac{\langle\omega_{de}\rangle}{\omega}>>\frac{T_e}{T_h}$. In this regime, the dispersion relation is given by Eq. (3.38) with the $\langle G\rangle$ term ignored, and stability is determined by the sign of the discriminant. This limit will be investigated in more details for the point dipole equilibrium in Sec. V.

For completeness we also examine the case of equal hot and background pressures with $\beta_h \sim \beta_b \sim 1$. Recalling the frequency ordering, this limit requires $\frac{n_{0h}T_e}{p_{0b}}\sim\frac{T_e}{T_h}<<\frac{\langle\omega_{de}\rangle}{\omega}$. The dispersion relation then reduces to

$$\frac{\omega^2}{\langle\omega_{de}\rangle^2}=\frac{(\gamma-d)\left(1+\frac{1}{2}d\langle\beta_b\rangle+\frac{\langle\beta_h\rangle}{2}\langle I\rangle\right)}{\langle b\rangle\left(1+\frac{1}{2}\gamma\langle\beta_b\rangle+\frac{\langle\beta_h\rangle}{2}\langle I\rangle\right)}, \tag{3.40}$$

with stability determined by the signs of three terms on the right hand side. Section V will also investigate this limit in more detail for a point dipole, for which $\gamma > d$ always, so only sign changes in the numerator need to be considered.

3.4.B. Resonant hot electron drift effects on stability.

It is also of interest to examine how weak hot electron drift resonance effects change stability boundaries. We examine these effects by retaining the imaginary parts of $\langle G \rangle$, $\langle H \rangle$, $\langle F \rangle$, and $\langle I \rangle$. Since the imaginary parts of the hot electron coefficients are much smaller than the real ones, we may examine resonant effects perturbatively by writing $\omega = \omega_0 + \omega_1$, where $\omega_0 >> |\omega_1|$ is the zero order solution to Eq. (3.38) with real coefficients, and ω_1 is the small complex correction due to the hot drift resonance. Due to its small size, ω_1 cannot stabilize a zero order instability or significantly affect the stability boundary, so we only look at real solutions to the dispersion relation by considering real ω_0 and ignoring the real part of ω_1. Moreover, without drift reversal, a weak drift resonance for $l > 0$ is possible only for positive wave frequencies so we require $\omega_0 > 0$. We need only consider $l > 0$ since reality requires $-\omega^*$, $-l$ be a solution if ω, l is a solution.

The full details of obtaining the expressions for imaginary parts of hot electrons coefficients are provided in Appendix 3.C. Here we note that to the required order they can be written as

$$\langle G_{res}\rangle = -\Delta\frac{2p_{0b}T_h}{n_{0h}T_e^2}\Lambda_1, \qquad \langle H_{res}\rangle = \Delta\frac{\omega_0}{\langle\omega_{de}\rangle}\frac{2p_{0b}}{n_{0h}T_e}\Lambda_2,$$
$$\langle F_{res}\rangle = \Delta\frac{\omega_0}{\langle\omega_{de}\rangle}\frac{2p_{0b}}{n_{0h}T_e}\Lambda_3 \quad \text{and} \quad \langle I_{res}\rangle = \Delta\frac{\omega_0^2}{\langle\omega_{de}\rangle^2}\frac{2p_{0b}}{p_{0h}}\Lambda_4, \tag{3.41}$$

with Δ defined by

$$\Delta = \frac{i\sqrt{\pi}\omega_{*h}\left(1-\frac{3}{2}\eta_h\right)}{\langle\omega_{de}\rangle}\frac{n_{0h}T_e}{2p_{0b}}\sqrt{\frac{\omega_0}{\langle\omega_{de}\rangle}}\left(\frac{T_e}{T_h}\right)^{5/2}, \tag{3.42}$$

and the positive geometrical coefficients defined by

$$\Lambda_1 = \frac{1}{2}\langle\omega_{dh}\rangle^{3/2}\left\langle\frac{B_0}{\overline{B}}\int_0^{\overline{B}/B_0}\frac{d\lambda}{\omega_D^{3/2}\sqrt{1-\lambda B_0/\overline{B}}}\right\rangle,$$
$$\Lambda_2 = \frac{\langle\omega_{dh}\rangle^{5/2}}{2\overline{B}^2\langle B_0^{-2}\rangle}\left\langle\frac{B_0}{\overline{B}}\int_0^{\overline{B}/B_0}d\lambda\frac{\lambda\oint d\tau(\overline{B}/B_0)/\oint d\tau}{\omega_D^{5/2}\sqrt{1-\lambda B_0/\overline{B}}}\right\rangle,$$
$$\Lambda_3 = \frac{\langle\omega_{dh}\rangle^{5/2}}{2\overline{B}^2\langle B_0^{-2}\rangle}\left\langle\int_0^{\overline{B}/B_0}\frac{\lambda d\lambda}{\omega_D^{5/2}\sqrt{1-\lambda B_0/\overline{B}}}\right\rangle,$$
$$\Lambda_4 = \frac{\langle\omega_{dh}\rangle^{7/2}}{2\overline{B}^4\langle B_0^{-2}\rangle^2}\int_0^{\overline{B}/B_0}d\lambda\frac{\lambda^2\oint d\tau(\overline{B}/B_0)/\oint d\tau}{\omega_D^{7/2}\sqrt{1-\lambda B_0/\overline{B}}}.$$

where $\langle\omega_{dh}\rangle = \langle\omega_{de}\rangle T_h/T_e$.

The expression for the first order complex correction for the fully electromagnetic case is quite cumbersome. To understand the procedure of obtaining ω_1, we schematically represent the general zero order dispersion relation as

$$A\frac{\omega_0^2}{\langle\omega_{de}\rangle^2} + B\frac{\omega_0}{\langle\omega_{de}\rangle} + C = 0,$$

with A, B and C are the real coefficients of corresponding powers of $\omega/\langle\omega_{de}\rangle$ in Eq. (3.38) and given by

$$A=\left[\langle b\rangle\left(1+\tfrac{1}{2}\gamma\langle\beta_b\rangle+\frac{\langle\beta_h\rangle}{2}\langle I\rangle\right)+\frac{\langle\beta_b\rangle}{2}\left(\frac{n_{0h}T_e}{p_{0b}}\right)^2(1-\langle H\rangle)(1-\langle F\rangle)\right]$$

$$B=\frac{n_{0h}T_e}{p_{0b}}\left[\left(1+\frac{d\ln n_{0h}}{d\ln V}\right)\left(1+\tfrac{1}{2}\gamma\langle\beta_b\rangle+\frac{\langle\beta_h\rangle}{2}\langle I\rangle\right)-\frac{\langle\beta_b\rangle}{2}(\gamma-d)(2-\langle H\rangle-\langle F\rangle)\right],$$

$$C=-(\gamma-d)\left(1+\tfrac{1}{2}d\langle\beta_b\rangle+\frac{\langle\beta_h\rangle}{2}\langle I\rangle\right),$$

where the contribution from the term involving $\langle G\rangle$ is always small by at least $T_e << T_h$.

The general zero order stability boundary is described by the real solution of the preceding equation. The expression for the first order imaginary correction can be written as

$$\frac{\omega_1}{\omega_0}=\Delta NK, \tag{3.43}$$

where

$$\begin{aligned}K=&\kappa^2\left[\alpha^2\ (1-\langle H\rangle)(1-\langle F\rangle)-\alpha(2-\langle H\rangle-\langle F\rangle)+1\right]\Lambda_4\\&+\kappa\left\{\alpha\left[\Lambda_2(1-\langle F\rangle)+\Lambda_3(1-\langle H\rangle)\right]-(\Lambda_2+\Lambda_3)\right\}+\Lambda_1,\end{aligned} \tag{3.44}$$

and

$$N=\frac{\left(1+\frac{1}{2}\gamma\langle\beta_b\rangle+\frac{1}{2}\langle\beta_h\rangle\langle I\rangle\right)}{A+\frac{\langle\omega_{de}\rangle}{2\omega_0}B} \tag{3.45}$$

with

$$\kappa=\frac{\langle\beta_b\rangle(\gamma-d)}{2\left(1+\frac{1}{2}\gamma\langle\beta_b\rangle+\frac{1}{2}\langle\beta_h\rangle\langle I\rangle\right)}\ \text{and}\ \alpha=\frac{\omega_0 n_{0h}T_e}{\langle\omega_{de}\rangle p_{0b}(\gamma-d)}. \tag{3.46}$$

The sign of the Eq. (3.43) determines if plasma is weakly unstable. In our Z-pinch investigation, we have extensively evaluated all possible cases and requirements for this weak resonant instability. Here we will focus on three cases: electrostatic background, electromagnetic with $\beta_h \sim \beta_b \sim 1$, and the high β_h electromagnetic case $\beta_h >> \beta_b \sim 1$ for the point dipole equilibrium.

For the electrostatic background case $\beta_b << \beta_h \sim 1$, $\kappa \approx 0$, and in the absence of drift reversal $K > 0$, with ω_0 the solution of the simplified zero order dispersion relation given by Eq. (3.39). Equation (3.39) is a quadratic with real coefficients, and for the resonant modes to be of interest it must have two real stable roots. If $d > \gamma$, then both roots are positive if $d\ln n_{0h}/d\ln V < -1$, in which case the resonance is always unstable. Both roots are negative if $d\ln n_{0h}/d\ln V > -1$, in which case there is no resonance and the plasma is stable. Therefore, if $d > \gamma$ we also require $d\ln n_{0h}/d\ln V > -1$ to be completely stable due to charge uncovering effects. If $d < \gamma$, then there is always one positive root, which permits a resonance, and the stability of the region depends only on the signs of Δ and the numerator of N. For $d < \gamma$ case stability requires

$$\left(1+\tfrac{1}{2}\langle\beta_h\rangle\langle I\rangle\right)\left(\frac{d\ln n_{0h}}{d\ln\psi}-\frac{3}{2}\frac{d\ln T_h}{d\ln\psi}\right)\le 0, \tag{3.47}$$

where the sign of $\langle I\rangle$ depends on sign of $d\ln p_{0h}/d\ln\psi$ and the details of the dipole magnetic field. For the point dipole considered in the next section, the sign of $\langle I\rangle$ depends only on sign of $d\ln p_{0h}/d\ln\psi$ and the plasma beta.

If we consider the electromagnetic case, with $\beta_h \sim \beta_b \sim 1$, then the α or charge uncovering terms become negligible, N reduces to $N = 1/\langle b\rangle > 0$, all Λ_j terms are positive without the drift reversal, and the expression for K becomes

$$K = \kappa^2\Lambda_4 - (\Lambda_2+\Lambda_3)\kappa + \Lambda_1 = \Lambda_4\left(\kappa - \frac{\Lambda_2+\Lambda_3}{2\Lambda_4}\right)^2 + \Lambda_1 - \frac{(\Lambda_2+\Lambda_3)^2}{4\Lambda_4}.$$

In this limit, stability depends on the sign of ΔK. If

$$d\ln n_{0h}/d\ln\psi \le \tfrac{3}{2}\, d\ln T_h/d\ln\psi,$$

then a sufficient condition for stability is $\Lambda_1 \geq (\Lambda_2 + \Lambda_3)^2 / 4\Lambda_4$.

If we allow $\beta_h >> 1 \sim \beta_b$, then $\alpha \sim 1$ and the general result of Eq. (3.43) must be considered. A sufficient condition for stability can then be seen to be $\gamma > d$, $\left(1 + \frac{1}{2}\gamma\langle\beta_b\rangle + \frac{1}{2}\langle\beta_h\rangle\langle I\rangle\right) > 0$, $\langle F\rangle < 1$, $\langle H\rangle < 1$, and $d\ln n_{0h} / d\ln\psi \leq \frac{3}{2} d\ln T_h / \ln d\psi$. However, more detailed results require a specific dipole equilibrium. In the next section we consider this high β_h case further, as well as the situations already discussed, for the point dipole equilibrium[17]. Their point dipole model allows us to simplify the computational aspect of our analysis, while retaining enough features of the general dipole geometry to be of interest to LDX.

3.5 Point Dipole Application

In the previous section we derived and discussed the dispersion relation for interchange stability in general dipole geometry. Unlike the Z-Pinch, the dipole dispersion relation involves flux surface averages of various geometrical quantities, making it difficult to usefully discuss stability without numerical work and a specific dipole equilibrium. To obtain semi-analytical results we adopt the point dipole equilibrium found by writing the poloidal magnetic flux in the separable form given by

$$\psi(r,u) = \psi_0 h(u) \left(\frac{r_0}{r}\right)^a, \tag{3.48}$$

where $u = \cos\theta$ and $R = r\sin\theta$, with r and θ spherical coordinates and θ measured from the axis of symmetry[17]. Here, ψ_0 and r_0 are normalization constants and a is a parameter between zero and one to be determined. The spatial behavior of ψ is governed by Grad-Shafranov equation, which for the choice of Eq. (3.48) and

$$p(\psi) = p_0(\psi/\psi_0)^{2+4/a} \tag{3.49}$$

can be rewritten as an ordinary differential equation for $h(u)$:

$$\frac{d^2h}{du^2} = -\frac{a(a+1)}{(1-u^2)}h - a(a+2)\beta h^{1+4/a}, \tag{3.50}$$

where $\beta = \frac{2\mu_0 p_0 r_0^4}{a^2\psi_0^2}$, with p_0 being a normalization constant. Solving the preceding equation for $h(u)$ determines the eigenvalue $a = a(\beta)$, with $a \to 1$ for $\beta \to 0$ and $a \to 0$ for $\beta \to \infty$. For this model the local beta, defined in Sec. II, is only a function of poloidal angle and is given by $\beta_0 \equiv \beta a^2 h^{4/a} / \left[\left(\frac{d\ln h}{du}\right)^2 + \frac{a^2}{1-u^2}\right]$.

Using this separable form we can express the spatial dependence of all required quantities in terms of ψ, $h(u)$, and its derivatives, and evaluate all of the flux surface and trajectory averages.

We begin by addressing the issue of drift reversal in point dipole geometry, which requires the evaluation of ω_D. Figures 3.1 present graphs of $-\vec{v}_d \cdot \nabla\zeta\left(2lT_h/mv^2\right)$, which when trajectory averaged becomes ω_D, given by Eq. (3.27). We plot this expression as a function of u for different values of β and λ.

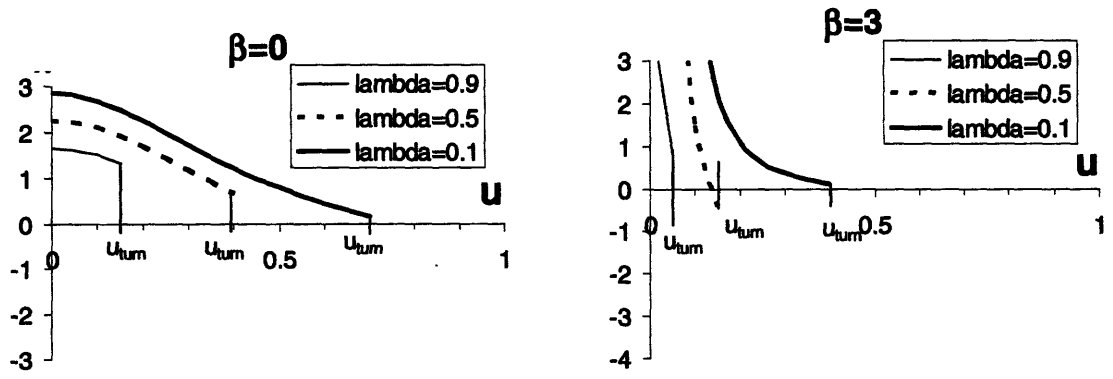

(a) (b)

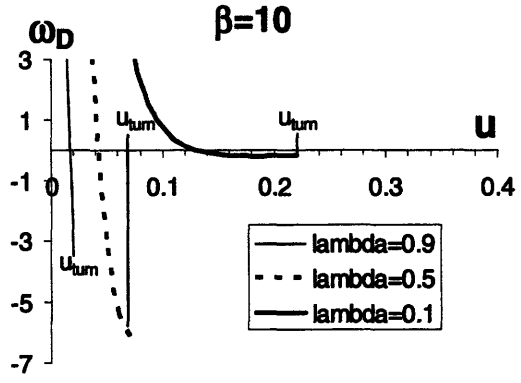

(c)

Figures 3.1 (a)-(c): Expression $-\vec{v}_d \cdot \nabla\zeta\left(2lT_h / mv^2\right)$ as a function of u for different values of β and λ. The bold solid line is λ=0.1, the thin solid line is λ=0.9, and the dotted is λ=0.5

From the graphs we can see that the integrand can become negative. However, even at large β, the particles do not spend enough time in the regions with reversed magnetic drift to make ω_D, the effective trajectory averaged drift, negative. As a result, drift reversal is not possible in point dipole geometry.

We next proceed to the evaluation of the hot electron coefficients I, F, and H, as well as their trajectory averages entering in the dispersion relation. Figures 3.2 illustrate the dependencies of I, F, and H on u for different values of β, where I is normalized to $d\ln p_{0h} / d\ln\psi$, while F and H are normalized to $d\ln n_{0h} / d\ln\psi$.

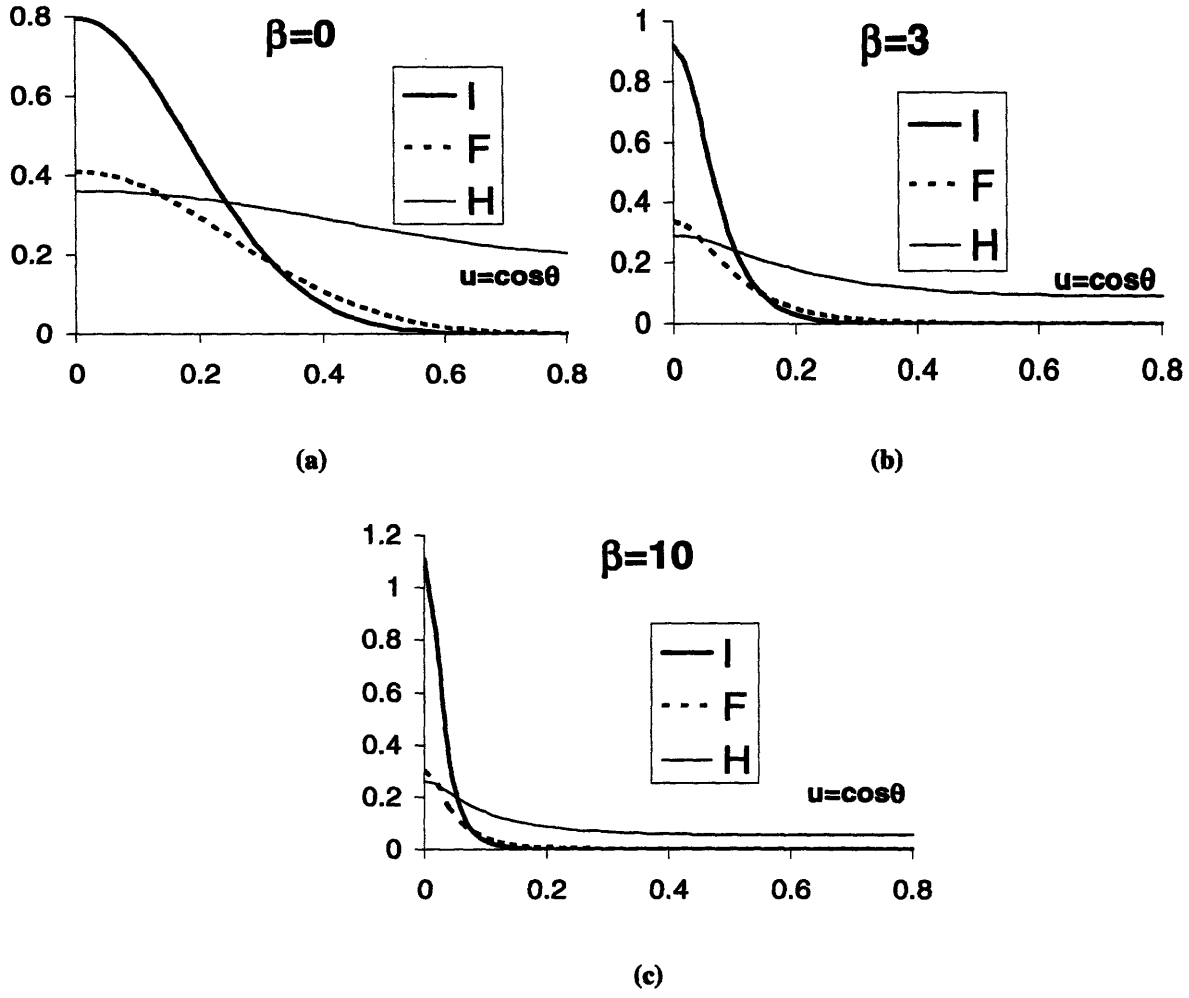

Figures 3.2 (a)-(c): Normalized hot electron coefficients *I*, *F*, and *H* as a function of *u* for different values of β. The bold solid curve is the coefficient *I*, normalized to $d\ln p_{0h}/d\ln\psi$, while the dotted curve is the coefficient *F* and the thin solid curve is the coefficient *H*, both normalized to $d\ln n_{0h}/d\ln\psi$.

As we can see from the plots, all three normalized coefficients are positive at all possible u, so their flux surface averages will also be positive, as confirmed in Fig. 3.3, where we plot $\langle I \rangle$, $\langle F \rangle$, and $\langle H \rangle$ as a function of β. We take $d\ln n_{0h}/d\ln\psi = 1$ and $\eta_h = 0$, so that $\langle I \rangle$, $\langle F \rangle$, and $\langle H \rangle$ are normalized to $d\ln p_{0h}/d\ln\psi$ and $d\ln n_{0h}/d\ln\psi$, respectively.

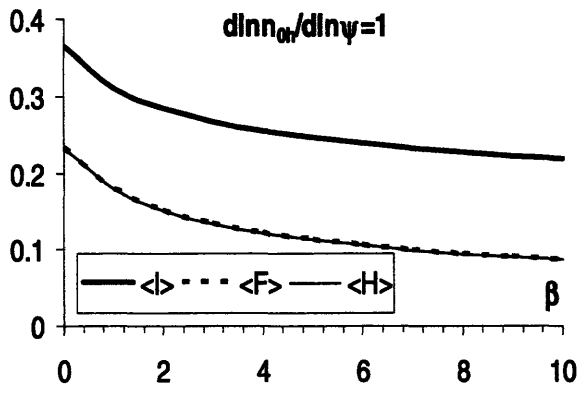

Figure 3.3: Flux surface averages of normalized hot electron coefficients *I*, *F*, and *H* as a function of β with $d\ln n_{oh}/d\ln\psi=1$ and $\eta_h=0$ for normalization. The bold solid line is <*I*>, the dotted line is <*F*>, and the thin solid line is <*H*>.

As we can see from the plot, the normalized flux surface average of I is positive, and both normalized $\langle F\rangle$ and $\langle H\rangle$ are also positive as well as less than unity. It is also obvious from Fig. 3.3 that $\langle H\rangle \approx \langle F\rangle$, and therefore the expression for K, which describes the resonant particle effects, can be approximately written as

$$K \approx \Lambda_4\{\kappa[\alpha(1-\langle H\rangle)-1]+(\Lambda_2+\Lambda_3)/2\Lambda_4\}^2+\Lambda_1-\frac{(\Lambda_2+\Lambda_3)^2}{4\Lambda_4}.$$

As a result, only if $\Lambda_1-(\Lambda_2+\Lambda_3)^2/4\Lambda_4$ becomes negative, can K change sign, an observation we will return to, when the resonant effects of hot electrons are addressed later in the section.

Next, we turn our attention to analyzing the lowest order stability condition, which ignores the resonant particle effects and for the general case is described by the dispersion relation of Eq. (3.38). It is convenient to illustrate this analysis with plots of d as a function of β. To do so, we use the expression that relates the total pressure gradient to the hot and the background pressure gradients, namely

$$\frac{d\ln p}{d\ln\psi}=2+\frac{4}{a}=\frac{\langle\beta_h\rangle}{\langle\beta_0\rangle}\frac{d\ln p_{0h}}{d\ln\psi}+\frac{\langle\beta_b\rangle}{\langle\beta_0\rangle}\frac{d\ln p_{0b}}{d\ln\psi}, \tag{3.51}$$

where for this point dipole model the total pressure is given by Eq. (3.49). Notice that if we assume equal background and hot electron pressure profiles and use $d\ln V/d\ln\psi=-(1+3/a)$, we find that lowest order stability is always satisfied since $d=(2a+4)/(a+3)<\gamma=5/3$.

For the electrostatic case with $\beta_b \ll \beta_h \sim 1$, Eq. (3.51) reduces to $2+4/a \approx d\ln p_{0h}/d\ln\psi$, which when substituted in the dispersion relation given by Eq. (3.39) yields

$$\left(1+\frac{\langle\beta_h\rangle}{2}\langle I\rangle\right)\left[\frac{\omega^2}{\langle\omega_{de}\rangle^2}\langle b\rangle+\frac{n_{0h}T_e}{p_{0b}}\frac{\omega}{\langle\omega_{de}\rangle}\left(1-\frac{2a+4}{a+3}\frac{1}{1+\eta_h}\right)-(\gamma-d)\right]=0,$$

where we used $d\ln V/d\ln\psi=-(1+3/a)$ and $d\ln n_{0h}/d\ln\psi=(d\ln p_{0h}/d\ln\psi)/(1+\eta_h)$. The stability boundary is described by $d\le\gamma+\frac{\left(1-\frac{2a+4}{a+3}\frac{1}{1+\eta_h}\right)^2}{4\langle b\rangle(p_{0b}/n_{0h}T_e)^2}$ and can be graphically represented as in Fig. 3.4,

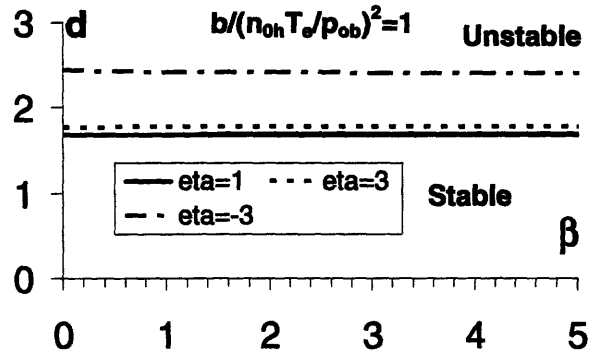

Figure 3.4: Stability regions for different values of η_h with $b(p_{0b}/n_{0h}T_e)^2=1$. The bold solid curve is $\eta_h=1$, which coincides with the thin solid line $d=\gamma$. The dash-dotted line is $\eta_h=-3$ and the dotted line is $\eta_h=3$.

where the $\eta_h = 1$ and $d = \gamma$ curves overlap. As we can see from the graph, the charge uncovering effects due to hot electrons are stabilizing, and allow achieving stability with d above γ when η_h is kept negative.

Next, we consider fully electromagnetic case with $\beta_h >> \beta_b \sim 1$, so that the total plasma pressure remains mostly contained in the hot electrons. It follows from Eq. (3.51) that $d \ln p / d \ln p_{0h} \approx 1$, and as a result the expression for $\langle I \rangle$, which is dependent on $d \ln p_{0h} / d \ln \psi$ is positive. In addition the expressions for $1 + \frac{1}{2}\gamma\langle \beta_b \rangle + \frac{1}{2}\langle \beta_h \rangle \langle I \rangle$ and the coefficient A given before Eq. (3.43), with $(1 - \langle H \rangle)(1 - \langle F \rangle) \approx (1 - \langle H \rangle)^2$ are positive. The dispersion relation for this case is given by Eq. (3.38) without the small $\langle G \rangle$ term. The stability boundary is illustrated in Figs. 3.5 where d is plotted as a function of β for different values to η_h,

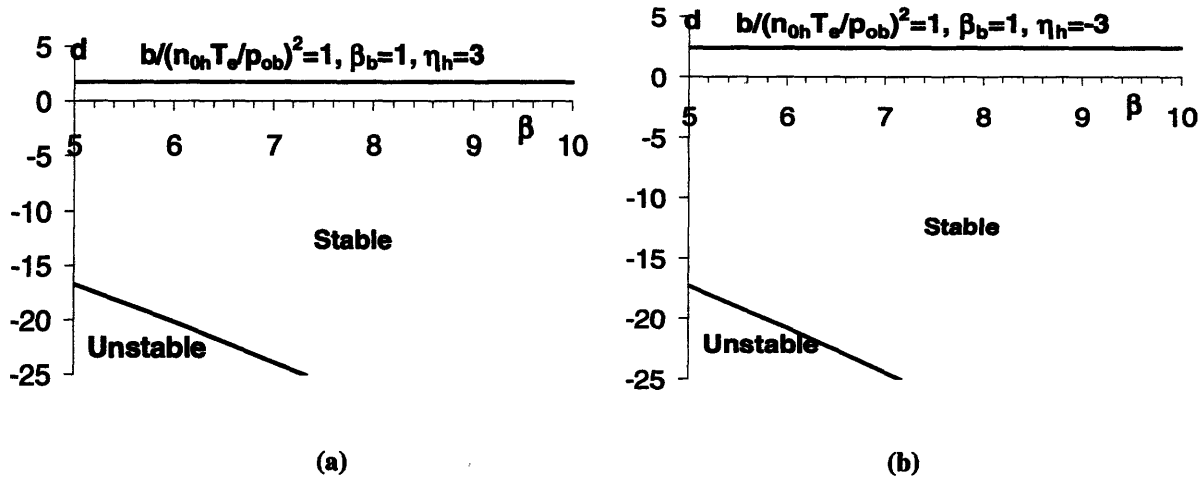

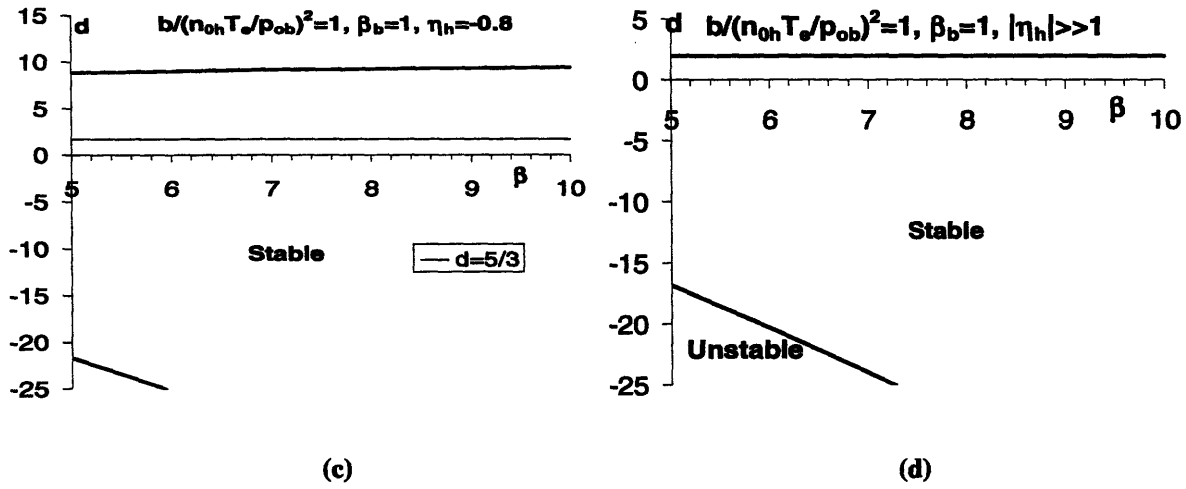

(c) (d)

Figures 3.5 (a)-(d): Stability regions for different values of η_h with β_b =1 and $b(p_{0b}/n_{0h}T_e)^2$=1. The thin solid line is d=γ. In figures (a), (b), and (d) it overlaps with the top solid curve.

and where the $d=\gamma$ curve overlaps with the top solid curve with the exception of the $\eta_h=-0.8$ case. As can be seen from the graphs, stability is improved in the vicinity of $\eta_h=-1$, but otherwise is rather insensitive to changes in η_h. The $b(p_{0b}/n_{0h}T_e)^2$ parameter does not affect the stability boundary significantly. When increased (decreased), it slightly shifts the two curves together (apart), thereby decreasing (increasing) the stability region. The graphs in Figs. 3.5 are only valid for $\beta \approx \beta_h >> \beta_b \sim 1$, that is above about $\beta=5$. For lower β, the stability condition is given by Fig. 3.4 if $\beta_b << \beta_h \sim 1$ or will be discussed shortly for $\beta_h \sim \beta_b \sim 1$.

It is also of some interest to take the hot and background pressure gradients as equal, so that Eq. (3.51) reduces to $2+4/a = d\ln p_{0h}/d\ln\psi = d\ln p_{0b}/d\ln\psi$. For this special case $d<\gamma$ and therefore A and C as given before Eq. (3.43), are positive and negative, respectively. Consequently, the plasma is always stable in the absence of resonant particles effects.

For the case of $\beta_h \sim \beta_b \sim 1$ the dispersion relation is given by Eq. (3.40) and the total plasma pressure is split between the background and hot particles. If, for example,

$\langle\beta_b\rangle=\langle\beta_h\rangle=\langle\beta_0\rangle/2$, then Eq. (3.51) reduces to $4(1+2/a)=d\ln p_{0h}/d\ln\psi+d\ln p_{0b}/d\ln\psi$, and it follows that

$$\frac{d\ln p_{0h}}{d\ln\psi}=4\left(1+\frac{2}{a}\right)-\left(1+\frac{3}{a}\right)d\,.$$

From Eq. (3.40), the stability boundary is determined by the signs of three expressions: $\gamma-d$, the numerator $1+\frac{1}{2}d\langle\beta_b\rangle+\frac{\langle\beta_h\rangle}{2}\langle I\rangle$, and the denominator $1+\frac{1}{2}\gamma\langle\beta_b\rangle+\frac{\langle\beta_h\rangle}{2}\langle I\rangle$, that are shown in Fig. 3.6. Unlike the previous two cases the stability boundaries are independent of η_h.

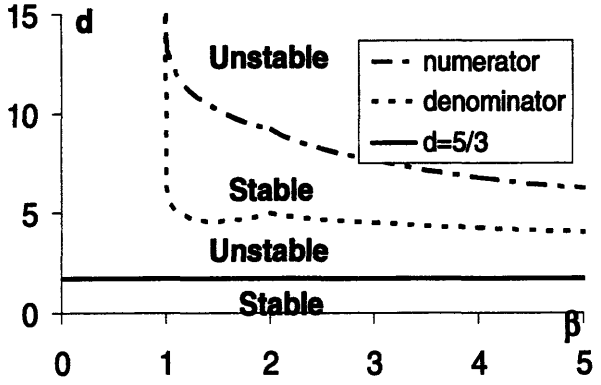

Figure 3.6: Stability regions for $<\beta_b>=<\beta_h>=<\beta_0>/2$. The bold solid curve is $d=\gamma$, the dash-dotted line is $1+d<\beta_b>/2+<I><\beta_h>/2=0$, the dotted line is $1+\gamma<\beta_b>/2+<I><\beta_h>/2=0$.

As we can see from the graph, $d<\gamma$ is expected to be the only experimentally accessible stability region, since the second stability region does not cover $\beta<1$, depends sensitively on $\langle\beta_h\rangle/\langle\beta_b\rangle$ and does not exist in the absence of hot electrons.

Next we consider the resonant hot electron effects that determine what we refer to as the first order stability boundary. We note that these effects are weak, and therefore cannot stabilize the lowest order instability, but can potentially destabilize the zero order stable regions. Recall

that resonant particle stability is determined by the sign of ω_1, which is given by Eq. (3.43), and depends on the signs of ω_0, Δ, N, and K. Since the expression for ω_0 is quadratic with real coefficients, in the stable regions it will have two real roots. Only positive roots can lead to a hot electron resonance with the wave, since otherwise the denominator in the expressions $\langle I \rangle$, $\langle F \rangle$, and $\langle H \rangle$, as given in Eq. (3.35), will not vanish. Consequently, stable regions with two negative real roots will remain stable due to the absence of resonance. Moreover, the lowest order stable regions with two positive roots will always become weakly unstable, regardless of the signs of Δ or K. This behavior occurs because of the denominator of N, which can be written as $A+\frac{\omega_{de}}{2\omega_0}B=\pm\frac{\omega_{de}}{2\omega_0}\sqrt{B^2-4AC}$. As both signs are present there will always be one unstable root. In the lowest order stable regions with one positive and one negative root, only the positive root can lead to a resonant instability, and the condition for it will then be determined by the signs of N, Δ, and K. We will first concentrate on the sign of the latter.

As we have discussed earlier in this section, the sign of K depends on the sign of $\Lambda_1-(\Lambda_2+\Lambda_3)^2/4\Lambda_4$. So we present the graph of $\Lambda_1-(\Lambda_2+\Lambda_3)^2/4\Lambda_4$ as a function of β in Fig. 3.7.

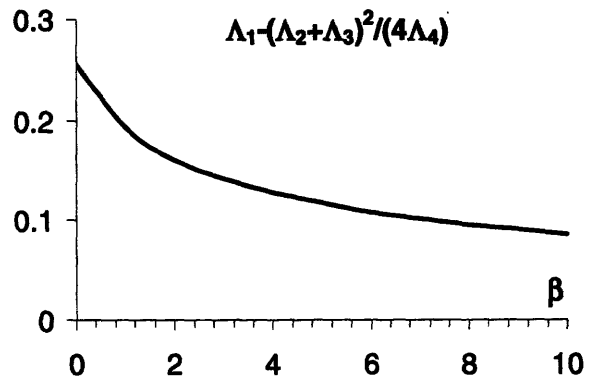

Figure 3.7: Graph of Λ_1-$(\Lambda_2+\Lambda_3)^2/(4\Lambda_4)$ vs. β.

The graph shows that this expression and, as a consequence, the expression for K, are always positive. So the condition for weak resonant stability in the regions of interest depends only on the signs of Δ and the numerator of N, which are considered next for the three different cases of beta orderings.

For the electrostatic background case of $\beta_b << \beta_h \sim 1$, first order or resonant particle stability requires

$$\frac{d\ln n_{0h}}{d\ln V} = -\frac{2(2+a)}{(a+3)(1+\eta_h)} > -1$$

if $d > \gamma$, as discussed in the previous section. This is the condition for the lowest order stable region to have two negative real roots and it is satisfied when $\eta_h < -1$ or $\eta_h > (a+1)/(a+3) > 1/3$. If $d < \gamma$, then the lowest order stable region has only one real positive root, and the first order stability is given by Eq. (3.47). For this beta ordering $\left(1+\frac{1}{2}\langle\beta_h\rangle\langle I\rangle\right) > 0$, so the plasma will be stable to a hot electron resonant instability if $d\ln n_{0h}/d\ln\psi \le \frac{3}{2} d\ln T_h/d\ln\psi$. This condition can also be written as $(d\ln p_{0h}/d\ln\psi)\left(1-\frac{3}{2}\eta_h\right)/(1+\eta_h) \le 0$ and is satisfied when $\eta_h < -1$ or $\eta_h > 2/3$. Thus, Fig. 3.4 suggests that to avoid hot electron resonance destabilization we need to avoid operation with $-1 \le \eta_h < 2/3$.

For electromagnetic case of $\beta_b \sim \beta_h \sim 1$, the zero order stability boundary is independent of η_h, and stable regions always have one positive and one negative root. Therefore, as discussed in the previous section, the resonant particle stability depends only on the sign of Δ and requires $d\ln n_{0h}/d\ln\psi \le \frac{3}{2} d\ln T_h/d\ln\psi$, which as before is satisfied when $\eta_h < -1$ or

$\eta_h > 2/3$. So as in the electrostatics case, the regions of operation with $-1 \le \eta_h < 2/3$ should be avoided.

For the electromagnetic case of $\beta_h >> \beta_b \sim 1$, we recall that the coefficient A, given before Eq. (3.43) is always positive, and the plasma will be resonant stable in the regions with $C > 0$ and $B > 0$, where it has two real negative roots. When $C < 0$ there is only one positive root, and the sign of Δ determines the stability, so $d \ln n_{0h} / d \ln \psi \le \frac{3}{2} d \ln T_h / d \ln \psi$ is required for stability.

In this high β_h case, unless $\eta_h \to -1$, the lowest order stability boundary very closely coincides with the $C = 0$ curves. As a result, except for this special case, resonant electron stability requires $d \ln n_{0h} / d \ln \psi \le \frac{3}{2} d \ln T_h / d \ln \psi$.

For the special case of $\eta_h \to -1$, the stability condition is presented in Fig. 3.8, where the signs of B and C are plotted as a function of β, and we also remind readers of the lowest order stability boundaries, which are shown in faint grey.

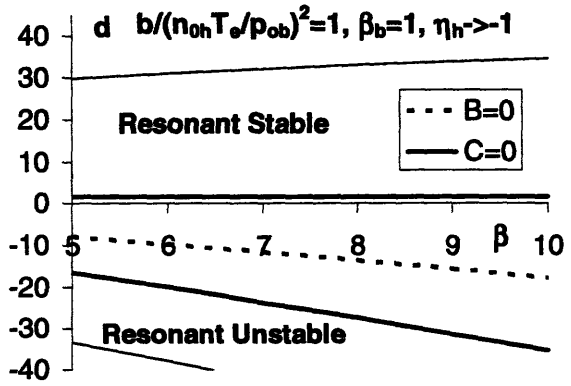

Figure 3.8: Stability regions for η_h->-1 with β_b =1 and $b(p_{0b}/n_{0b}T_e)^2$=1. The dotted line is B=0, two bold solid lines are C=0 and thin solid lines are the lowest order boundaries as shown in Figs. 3.2.

In this graph, the two solid lines bound the region with $C<0$, where the plasma is resonantly stable if $d\ln n_{0h}/d\ln\psi \le \frac{3}{2} d\ln T_h/d\ln\psi$. The region above the top solid line, but below the faint grey line has $C>0$ and $B>0$, and is always stable since the two lowest order roots are negative. The region below the bottom solid line and above the faint grey line has $C>0$ and $B<0$, and is always resonantly unstable since it has two positive roots.

We conclude this section by stressing, that keeping $d<\gamma$ and $d\ln n_{0h}/d\ln\psi \le \frac{3}{2} d\ln T_h/d\ln\psi$ is the best means of keeping the plasma stable. In special cases, these conditions can be relaxed, but more profile control is required.

3.6 Conclusions

We have investigated the effects of hot electrons on the interchange stability of a plasma confined by a dipole magnetic field and have obtained the general dispersion relation for arbitrary beta. The analysis of the stability boundary is dependent on the particular details of magnetic field, as well as the background and hot electron pressure, temperature and number density profiles. As a particular illustration of the preceding theoretical development, the dispersion relation is analyzed in detail for a point dipole equilibrium.

Our analysis indicates that it is impossible to have magnetic drift reversal in the point dipole, but it might become a concern in more general dipole geometry, in which case a strong instability would occur.

If resonant hot electron effects are neglected, we find that the general, experimentally achievable interchange stability condition normally remains close to $d<\gamma$. In a point dipole we

demonstrate that this condition can be improved and d can be allowed to exceed γ either in the case of an electrostatic background by keeping η_h negative, or in the electromagnetic case with $\beta_h >> \beta_b$ by keeping η_h close to negative unity.

Hot electron drift resonant effects result in small corrections to the mode frequency that can create weak instabilities in the stable regions. Usually this weak instability can be avoided by satisfying the condition $d \ln n_{0h} / d \ln \psi \leq \frac{3}{2} d \ln T_h / d \ln \psi$.

Chapter 4

Conclusions

In this thesis the effects of hot electrons on the interchange stability of a plasma confined by closed magnetic field lines was investigated. This work has been motivated by a desire to determine how interchange stability is modified by the presence of hot population due to electron cyclotron heating. Our study has demonstrated the key roles that hot electron magnetic drift reversal and the hot electron fraction and profiles will play in the Levitated Dipole Experiment. The results of this work are applicable to LDX and can be useful to other closed field line devices.

In Chapter 2, we first have developed the procedure for Z-pinch plasmas, which can be thought of as a linear approximation to a dipole. The simplicity of this geometry, while preserving the feature of closed field lines and allowing us to treat the diamagnetic and magnetic drifts as comparable, gave us the ability to understand the physics behind the destabilizing influences due to a hot electron population. In particular, our results yielded two different types of resonant hot electron effects that modify the usual ideal MHD interchange stability condition.

The first occurs when the magnetic field is an increasing function of radius and there is a critical pitch angle for which the magnetic drift of hot electrons reverses direction. This interaction between the wave and the particles with the pitch angles close to critical always causes instability for Maxwellian hot electrons. And as a result, stable operation is not possible for such a magnetic field profile.

When the drift reversal does not occur and resonant hot electron effects are neglected, we find that interchange stability can be enhanced compared to the usual MHD interchange condition by increasing the background plasma pressure as well as the gradient of the hot electron density for $\beta_h >> \beta_b \sim 1$. However, further increasing β_b beyond two or three, did not result in significant increases in stability region. When the hot electron drift effects are retained, they can potentially cause a weak resonant hot electron instability. This second destabilizing effect due to the hot electron drift resonance can be avoided by controlling the hot electron density and temperature profiles so that $rn'_{0h}/n_{0h} > 3rT'_h/2T_h$.

Geometry can be important in evaluating effects of hot electrons on a plasma interchange stability. Consequently, we extended our calculations to dipolar geometry in Chapter 3 and have obtained the general dispersion relation for arbitrary beta. The analysis of the stability boundary dependents on the details of magnetic field, background and hot electron pressure, temperature and number density profiles. To illustrate the application of the preceding theoretical development, we have the analyzed the dispersion relation for a point dipole equilibrium. Unlike the Z-pinch case, our analysis of a point dipole showed that it was impossible to have magnetic drift reversal. However, this may become an issue in more general dipole geometry or when the effects of anisotropic temperature due to ECRH are considered, in which case a strong instability would occur.

Without the resonant hot electron effects, the general, experimentally achievable interchange stability condition normally remains close to $d < \gamma$. In a point dipole geometry this condition could be improved and d could be allowed to exceed γ in the case of an electrostatic background by keeping η_h negative or in the electromagnetic case with $\beta_h >> \beta_b \sim 1$ by keeping η_h close to negative unity.

As in the Z-pinch case, the hot electron drift resonant effects in a dipole resulted in small corrections to the mode frequency that could create a weak instability in the interchange stable regions. This weak instability can be avoided by controlling the number density and temperature profiles of the hot electrons so they satisfy $d\ln n_{0h}/d\ln\psi \le \frac{3}{2} d\ln T_h/d\ln\psi$.

The work presented here can be expanded in many ways. As an example of a possibly interesting continuation we mention the investigation of anisotropic temperature effects of hot electrons on plasma stability. The ECRH tends to heat predominantly in the direction perpendicular to the magnetic field, and as a result the parallel and perpendicular temperatures are expected to different. The velocity space anisotropy may have a great impact, particularly if the ∇B_0 drift were to reverse. Another interesting problem that has been mentioned only in passing here is the stability of HEI modes in Z-pinch and dipolar geometry. These effects are of great interest to LDX community, since they depend on the hot electron fraction, as well as density profile and seem to be observed in LDX. Finally, the extension of the point dipole case to the particular dipolar geometry of LDX and the solution of the full integro-differential description would be useful to the LDX effort.

APPENDIX 2.A: EVALUATION OF HOT ELECTRON RESPONSE.

This appendix presents details of hot electron response expressions G, H and $s_h I$. Recall that the perturbed hot electron density and radial current are given by

$$\frac{n_{1h}}{n_{0h}} = \frac{1}{n_{0h}} \int f_{1h} d\vec{\mathbf{v}} = \frac{e\Phi}{T_h} G + \frac{B_{1\theta}}{B_0} H \tag{2.A1}$$

and

$$\frac{\mu_0 J_{1hr}}{ikB_0} = -\frac{\mu_0 e}{ikB_0} \int \mathrm{v}_r f_{1h} d\vec{\mathbf{v}} = \frac{e\Phi_1}{T_h} \frac{\beta_h}{2} H - \frac{B_{1\theta}}{B_0} s_h I , \tag{2.A2}$$

with f_{1h} given by Eq. (2.26). Thus, the expressions for G, H and $s_h I$ can be written as

$$G = 1 - \frac{2\omega_{*h}}{\sqrt{\pi}\omega_{kh}} \int_0^\infty dt e^{-t^2} \left[1 + \eta_h \left(t^2 - \frac{3}{2}\right)\right] \int_{-1}^{1} \frac{d\lambda}{D - \omega / t^2 \omega_{kh}} , \tag{2.A3}$$

$$H = \frac{2\omega_{*h}}{\sqrt{\pi}\omega_{kh}} \int_0^\infty dt e^{-t^2} t^2 \left[1 + \eta_h \left(t^2 - \frac{3}{2}\right)\right] \int_{-1}^{1} \frac{d\lambda \left(1 - \lambda^2\right)}{D - \omega / t^2 \omega_{kh}} , \tag{2.A4}$$

and

$$s_h I = \frac{\beta_h \omega_{*h}}{\sqrt{\pi}\omega_{kh}} \int_0^\infty dt e^{-t^2} t^4 \left[1 + \eta_h \left(t^2 - \frac{3}{2}\right)\right] \int_{-1}^{1} \frac{d\lambda \left(1 - \lambda^2\right)^2}{D - \omega / t^2 \omega_{kh}} , \tag{2.A5}$$

where $t^2 = m\mathrm{v}^2 / 2T_h$ and $D = (1+s)\lambda^2 + (1-s)$.

For $s < 1$ no drift reversal is possible and we can drop the $\omega / \omega_{kh} t^2$ term in the denominator due to $\omega << \omega_{kh}$, except for very small t, where slow electrons are resonant with the wave. Retaining this weak resonant effect the expressions for G, H and $s_h I$ become

$$G = 1 - \frac{\omega_{*h}(1 - \eta_h)}{\omega_{kh}} \int_{-1}^{1} \frac{d\lambda}{D} + G_{res} , \tag{2.A6}$$

$$H = \frac{\omega_{*h}}{2\omega_{kh}} \int_{-1}^{1} \frac{d\lambda\left(1-\lambda^2\right)}{D} + H_{res}, \text{ and} \tag{2.A7}$$

$$s_h I = \frac{3\beta_h \omega_{*h}(1+\eta_h)}{8\omega_{kh}} \int_{-1}^{1} \frac{d\lambda\left(1-\lambda^2\right)^2}{D} + \left(s_h I\right)_{res}, \tag{2.A8}$$

with

$$G_{res} = -i\frac{\sqrt{\pi}\omega_{*h}\left(1-\frac{3}{2}\eta_h\right)}{\omega_{kh}} \sqrt{\frac{\omega}{\omega_{kh}}} \int_{-1}^{1} \frac{d\lambda}{D^{3/2}}, \tag{2.A9}$$

$$H_{res} = i\frac{\sqrt{\pi}\omega_{*h}\left(1-\frac{3}{2}\eta_h\right)}{\omega_{kh}} \left(\frac{\omega}{\omega_{kh}}\right)^{3/2} \int_{-1}^{1} \frac{d\lambda\left(1-\lambda^2\right)}{D^{5/2}}, \text{ and} \tag{2.A10}$$

$$\left(s_h I\right)_{res} = i\frac{\sqrt{\pi}\omega_{*h}\left(1-\frac{3}{2}\eta_h\right)}{\omega_{kh}} \left(\frac{\omega}{\omega_{kh}}\right)^{5/2} \int_{-1}^{1} \frac{d\lambda\left(1-\lambda^2\right)^2}{D^{7/2}}. \tag{2.A11}$$

Observe that since D does not vanish for $s<1$, integrals over λ are easily evaluated, confirming that the non-resonant parts of expressions for G, H and $s_h I$ are all of order unity. As we noted at the beginning of Sec. 2.4, only the non-resonant part of $s_h I$ matters in the dispersion relation for $s<1$ to lowest order. Thus, ignoring the weak resonant effects, the hot electron response for $s<1$ is described only by $s_h I$, where I is given by Eq. (2.34).

The weak resonant effect of hot electrons for $s<1$ is calculated by evaluating the λ integrals in G_{res}, H_{res} and $\left(s_h I\right)_{res}$ to obtain the expressions given in Eqs. (2.40) – (2.41).

For $s>1$ there is always a critical pitch angle $|\lambda_0|<1$ for which D vanishes and therefore we must keep the ω term with $\mathrm{Im}\,\omega>0$ to satisfy causality. Evaluating the λ integral in the expression $s_h I$, Eq. (2.A8), we find

$$\int_{-1}^{1}\frac{d\lambda(1-\lambda^2)^2}{D-\omega/\omega_{kh}t^2}=-\frac{4}{3(1+s)^2}\left[(4+s)-3\int_{-1}^{1}\frac{d\lambda}{D-\omega/t^2\omega_{kh}}\right]=$$
$$=-\frac{4}{3(1+s)^2}\left\{(4+s)-3\left[-\frac{1}{\sqrt{s^2-1}}\ln\left(s+\sqrt{s^2-1}\right)+\frac{\pi i}{\sqrt{s^2-1}}\right]\right\}, \tag{2.A12}$$

where we have dropped $\omega/t^2\omega_{kh}$ order terms since they are much smaller than the leading imaginary term. As a result, the expression for $s>1$ is as given in Eq. (2.34).

Finally, we have to evaluate the expression for I at $s\to 1$. The vicinity of $s=1$ is the only region were the ω and t dependence of the integral

$$\int_{-1}^{1}\frac{d\lambda}{D-\omega/\omega_{kh}t^2}\underset{s\to 1}{\approx}\begin{cases}\dfrac{\pi}{\sqrt{2(1-s-\omega/t^2\omega_{kh})}}-1\ldots & s<1\\ \dfrac{\pi i}{\sqrt{2(s-1+\omega/t^2\omega_{kh})}}-1\ldots & s>1\end{cases} \tag{2.A13}$$

enters. The weak t dependence makes it awkward to do the t integrals exactly. However, to get the region about $s=1$ approximately correct, we evaluate the integrals in s_hI at $s=1$ getting

$$I=-\left[\frac{5}{4}-i\sqrt{\frac{\omega_{kh}}{\omega}}\frac{\sqrt{2\pi}\left(1+\frac{3}{2}\eta_h\right)}{(1+\eta_h)}\right], \tag{2.A14}$$

and then use the result to make an approximate fit that is independent of t. This procedure is equivalent to making the replacement

$$\int_{-1}^{1}\frac{d\lambda}{D-\omega/\omega_{kh}t^2}\underset{s\to 1}{\to}\begin{cases}\dfrac{\pi}{\sqrt{2(1-s-\sigma\omega/\omega_{kh})}}-1\ldots & s<1\\ \dfrac{\pi i}{\sqrt{2(s-1+\sigma\omega/\omega_{kh})}}-1\ldots & s>1,\\ \dfrac{\pi i}{\sqrt{2\sigma\omega/\omega_{kh}}}-1\ldots & s=1\end{cases} \tag{2.A15}$$

where

$$\sigma=\left[\frac{3(1+\eta_h)}{4\sqrt{\pi}(2+3\eta_h)}\right]^2.$$

Notice that if we were to repeat the same procedure for G and H as given by Eqs. (2.A3) – (2.A4) for $s>1$ and $s\to 1$, we would find that they are of the same order as $s_h I$ and therefore would not be significant in the dispersion relation.

APPENDIX 3.A: EVALUATION OF PERTURBED HOT ELECTRON DISTRIBUTION FUNCTION.

This appendix presents the detailed evaluation of the first order correction to the perturbed hot electron distribution function. We assume that the hot electrons satisfy the Vlasov equation and linearize the hot electron distribution function about its equilibrium by taking $f_h = f_{0h} + f_{1h} + \ldots$ with $f_{0h} = f_{0h}(\psi_*, E)$ satisfying Eq. (3.21) and f_{1h} satisfying Eq. (3.22). We follow the standard gyro-kinetic procedure[12,123] by removing the adiabatic response by introducing $g_1 = f_{1h} + \frac{e\Phi}{m}\frac{\partial f_{0h}}{\partial E}$ so that

$$\frac{df_{1h}}{dt} = \frac{dg_1}{dt} - \frac{d}{dt}\left(\frac{e\Phi}{m}\frac{\partial f_{0h}}{\partial E}\right) = -\frac{e}{m}\left(\nabla\Phi + \frac{\partial \vec{A}}{\partial t} - \vec{v}\times\vec{B}_1\right)\cdot\nabla_v f_{0h}, \tag{3.A1}$$

where $d/dt = \partial/\partial t + \vec{v}\cdot\nabla - \Omega_e \vec{v}\times\vec{B}_0\cdot\nabla_v$ is unperturbed Vlasov operator. Rewriting the above kinetic equation for g_1 yields

$$\begin{aligned}\frac{dg_1}{dt} &= \frac{\partial f_{0h}}{\partial E}\frac{d}{dt}\left(\frac{e\Phi}{m}\right) - \frac{e}{m}\left(\nabla\Phi + \frac{\partial \vec{A}}{\partial t} - \vec{v}\times\vec{B}_1\right)\cdot\nabla_v f_{0h} = \\ &= \frac{e}{m}\frac{\partial f_{0h}}{\partial E}\left(\frac{\partial\Phi}{\partial t} - \vec{v}\cdot\frac{\partial \vec{A}}{\partial t}\right) + \frac{\partial f_{0h}}{\partial \psi_*} R\hat{\zeta}\cdot\left(\nabla\Phi + \frac{\partial \vec{A}}{\partial t} - \vec{v}\times\vec{B}_1\right),\end{aligned} \tag{3.A2}$$

where $\frac{d}{dt}\left(\frac{\partial f_{0h}}{\partial E}\right) = 0$.

We denote the gyrophase independent and dependent portions of $g_1 = \bar{g}_1 + \tilde{g}_1$ with a bar and tilde, respectively. Next, we obtain the two equations for both parts of g_1. The equation for $\bar{g}_1$ is obtained by gyroaveraging Eq. (3.A2) using $E = v^2/2$, $\mu = v_\perp^2/2B_0$, and ϕ gyrophase on the left side. Recalling that $\tilde{g}_1$ is gyrophase periodic yields

$$\frac{\partial \bar{g}_1}{\partial t} + \vec{v}_\parallel\cdot\nabla\bar{g}_1 + \left\langle \vec{v}_\perp\cdot\nabla\tilde{g}_1\right\rangle_\phi = \frac{e}{m}\frac{\partial f_{0h}}{\partial E}\left(\frac{\partial\Phi}{\partial t} - \vec{v}_\parallel\cdot\frac{\partial \vec{A}}{\partial t}\right) + \frac{\partial f_{0h}}{\partial \psi_*} R\hat{\zeta}\cdot\left(\nabla\Phi + \frac{\partial \vec{A}}{\partial t} - \vec{v}_\parallel\times\vec{B}_1\right), \tag{3.A3}$$

with the gyrophase average defined by $\langle ... \rangle_\phi = \frac{1}{2\pi}\oint ... d\phi$. The equation for the gyrophase dependent part, $\tilde{g}_1$, is obtained by subtracting the preceding equation from Eq. (3.A2) to find

$$\frac{\partial \tilde{g}_1}{\partial t} + \vec{v}\cdot\nabla\tilde{g}_1 + \vec{v}_\perp\cdot\nabla\bar{g}_1 - \langle \vec{v}_\perp\cdot\nabla\tilde{g}_1\rangle_\phi + \Omega_e^{-1}\frac{\partial \tilde{g}_1}{\partial\phi} = -\vec{v}_\perp\cdot\left(\frac{e}{m}\frac{\partial f_{0h}}{\partial E}\frac{\partial \vec{A}}{\partial t} + R\frac{\partial f_{0h}}{\partial \psi_*}\vec{B}_1\times\hat{\zeta}\right). \quad (3.A4)$$

Using the orderings given by Eq. (3.20) we can expand $g_1 = g_1^0 + g_1^1 + \ldots$ and solve these two equations order by order. As a result, g_1^0 is gyrophase independent, since to lowest order Eq. (3.A4) gives

$$-\Omega_e\vec{v}\times\hat{b}\cdot\nabla_v g_1^0 = \Omega_e\frac{\partial \tilde{g}_1^0}{\partial\phi} = 0. \quad (3.A5)$$

In addition, Eq. (3.A3) to lowest order requires $\vec{v}_\parallel\cdot\nabla\bar{g}_1^0 = 0$, making $\bar{g}_1^0$ also a flux function to lowest order.

The solution of Eq. (3.A4) to next order gives us the equation for the first order gyrophase dependent part $\tilde{g}_1^1$, which we write as

$$\tilde{g}_1^1 = -\Omega_e^{-1}\vec{v}_\perp\times\hat{b}\cdot\left(\nabla\bar{g}_1^0 + \frac{e}{m}\frac{\partial f_{0h}}{\partial E}\frac{\partial \vec{A}}{\partial t} - \frac{B_\parallel}{B_0}\frac{\partial f_{0h}}{\partial \psi_*}\nabla\psi\right) \equiv \frac{\hat{b}}{\Omega_e}\times\vec{v}_\perp\cdot\vec{D}. \quad (3.A6)$$

With the help of the preceding equation we can calculate $\bar{g}_1^0$ from the next order version of Eq. (3.A3) by gyroaveraging and observing that

$$\left\langle \vec{v}_\perp\cdot\nabla\tilde{g}_1^1\right\rangle_\phi = \left\langle \vec{v}_\perp\cdot\nabla\left(\frac{\hat{b}}{\Omega_e}\right)\times\vec{v}\right\rangle_\phi\cdot\vec{D} + \left\langle \vec{v}_\perp\cdot\nabla\vec{D}\times\frac{\hat{b}}{\Omega_e}\cdot\vec{v}_\perp\right\rangle_\phi = \vec{v}_d\cdot\vec{D} + \frac{v_\perp^2}{2}\frac{\hat{b}}{\Omega_e}\cdot\nabla\times\vec{D},$$

with the magnetic drift velocity given by

$$\vec{v}_d = -\frac{\nabla\zeta}{\Omega_e B_0}\nabla\psi\cdot\left(\frac{v_\perp^2}{2}\nabla\ln B_0 + v_\parallel^2\vec{\kappa}\right).$$

Note that neither the curvature nor ∇B_0 have a $\nabla\zeta$ component.

Multiplying Eq. (3.A3) by $B_0 / v_{\parallel}$ and integrating over one complete poloidal circuit for the passing and one full poloidal bounce for the trapped particles to annihilate $\vec{v}_{\parallel} \cdot \nabla \bar{g}_1^1$ we then obtain Eq. (3.24).

APPENDIX 3.B: EVALUATION OF PERTURBED HOT ELECTRON NUMBER DENSITY AND RADIAL COMPONENT OF CURRENT.

In this appendix we evaluate the perturbed hot electron number density $n_{1h} = \int f_{1h} d\vec{v}$ and $\nabla\psi$ component of the current, $J_{1\psi} = -e\int v_\psi f_{1h} d\vec{v}$, where f_{1h} is given by Eqs. (3.23)-(3.25). It is clear that only the gyrophase independent part of g_1 contributes to n_{1h}, while only the gyrophase dependent part survives the integration in $J_{1\psi}$. Thus, the perturbed number density is given by

$$n_{1h} = \frac{e\Phi}{T_h} n_{0h} - \frac{e\Phi}{T_h}\int d\vec{v}\frac{f_{Mh}\left(\omega-\omega_{*h}^T\right)}{\left(\omega-\frac{mv^2}{2T_h}\omega_D\right)} + \int d\vec{v}\frac{mv^2}{2T_h}\frac{\lambda f_{Mh}\left(\omega-\omega_{*h}^T\right)\oint d\tau(Q_B/B_0\overline{B})/\oint d\tau}{\left(\omega-\frac{mv^2}{2T_h}\omega_D\right)}$$

where $\oint v_\parallel A_\parallel d\tau = 0$ since for an interchange mode $A_\parallel$ is up-down asymmetric.

The expression for $J_{1\psi} = -e\int v_\psi \tilde{g}_1 d\vec{v}$ may be rewritten as

$$J_{1\psi} = -\frac{mR}{2B_0}\int v_\perp^2 \nabla\zeta\cdot\left(\nabla\overline{g}_1 + \frac{ie\omega}{T_h} f_{Mh}\vec{A}\right)d\vec{v} = \frac{im}{2B_0}\int v_\perp^2\left(\frac{l}{R}\overline{g}_1 - \frac{e\omega}{T_h} f_{Mh} A_\zeta\right)d\vec{v}.$$

Before proceeding further we use the estimates $\overline{g}_1 \sim f_{Mh} e\Phi/T_h$ and $A_\zeta \sim A_\psi/l$ to compare the size of the terms in $J_{1\psi}$. Recalling Eqs. (3.30) and (3.31), we see that

$$\frac{f_{Mh}A_\zeta e\omega/T_h}{l\overline{g}_1/R} \sim \frac{\omega R A_\psi}{l^2\Phi} \sim 1/l^2 << 1.$$

Hence, for high mode number l we can ignore the A_ζ term compared with the $\overline{g}_1$ contribution. Therefore, the expression for $J_{1\psi}$ reduces to

$$J_{1\psi} = -\frac{e\Phi}{T_h}\frac{iml}{2R\overline{B}}\int d\vec{v}\frac{\lambda v^2 f_{Mh}\left(\omega-\omega_{*h}^T\right)}{\left(\omega-\frac{mv^2}{2T_h}\omega_D\right)} + \frac{im^2 l}{4T_h R\overline{B}}\int d\vec{v}\frac{\lambda^2 v^4 f_{Mh}\left(\omega-\omega_{*h}^T\right)\oint d\tau(Q_B/\overline{B}B_0)/\oint d\tau}{\left(\omega-\frac{mv^2}{2T_h}\omega_D\right)}.$$

If we also treat Q_B as a flux function to lowest order, then it can be taken outside of the $d\tau$ integrals in the expressions for n_{1h} and $J_{1\psi}$ to obtain Eqs. (3.33) and (3.34), respectively.

APPENDIX 3.C: EVALUATION OF IMAGINARY PARTS OF *G*, *H*, *F*, AND *I* TERMS.

This appendix presents the details of obtaining the weak hot electron drift resonance terms for the intermediate frequency regime with $\langle\omega_{dh}\rangle >> \omega >> \langle\omega_{de}\rangle$. Accounting for both signs of $v_{\|}$ gives $\int d\bar{v} \Rightarrow \int_0^{\bar{B}/B_0} \int_0^{\infty} \int_0^{2\pi} d\phi v^2 dv d\lambda (B_0/\bar{B})/2\sqrt{1-\lambda B_0/\bar{B}}$. We can then rewrite the full expressions for G, H, F, and I given by Eq. (3.35) at the end of Sec. 3.3. By evaluating the ϕ integral and defining $t = v\sqrt{m/2T_h}$ we obtain

$$
\begin{aligned}
G &= 1 - \frac{B_0}{\sqrt{\pi}\bar{B}} \int_0^{\bar{B}/B_0} \frac{d\lambda}{\sqrt{1-\lambda B_0/\bar{B}}} \int_0^{\infty} dt e^{-t^2} t^2 \frac{\omega - \omega_{*h}\left[1+\eta_h\left(t^2-\frac{3}{2}\right)\right]}{\omega - t^2\omega_D}, \\
H &= \frac{B_0\left\langle B_0^{-2}\right\rangle^{-1}}{\sqrt{\pi}\bar{B}^3} \int_0^{\bar{B}/B_0} d\lambda \frac{\lambda \oint d\tau (\bar{B}/B_0)/\oint d\tau}{\sqrt{1-\lambda B_0/\bar{B}}} \int_0^{\infty} dt e^{-t^2} t^4 \frac{\omega - \omega_{*h}\left[1+\eta_h\left(t^2-\frac{3}{2}\right)\right]}{\omega - t^2\omega_D}, \\
F &= \frac{\left\langle B_0^{-2}\right\rangle^{-1}}{\sqrt{\pi}\bar{B}^2} \int_0^{\bar{B}/B_0} \frac{\lambda d\lambda}{\sqrt{1-\lambda B_0/\bar{B}}} \int_0^{\infty} dt e^{-t^2} t^4 \frac{\omega - \omega_{*h}\left[1+\eta_h\left(t^2-\frac{3}{2}\right)\right]}{\omega - t^2\omega_D}, \\
I &= \frac{\left\langle B_0^{-2}\right\rangle^{-2}}{\sqrt{\pi}\bar{B}^4} \int_0^{\bar{B}/B_0} d\lambda \frac{\lambda^2 \oint d\tau (\bar{B}/B_0)/\oint d\tau}{\sqrt{1-\lambda B_0/\bar{B}}} \int_0^{\infty} dt e^{-t^2} t^6 \frac{\omega - \omega_{*h}\left[1+\eta_h\left(t^2-\frac{3}{2}\right)\right]}{\omega - t^2\omega_D}.
\end{aligned}
\tag{3.C1}
$$

To get the non-resonant, real parts of the expressions for G, H, F for $\omega << \langle\omega_{dh}\rangle \sim \omega_{*h}$, we simply neglect all ω dependence in the t integrals. Then we only need to evaluate the lowest order resonant contributions in the following expressions:

$$
\begin{aligned}
G &= 1-\frac{B_0\omega_{*h}(1-\eta_h)}{2\overline{B}}\int_0^{\overline{B}/B_0}\frac{d\lambda}{\omega_D\sqrt{1-\lambda B_0/\overline{B}}}+G_{res}\,,\\
H &= \frac{B_0\left\langle B_0^{-2}\right\rangle^{-1}\omega_{*h}}{4\overline{B}^3}\int_0^{\overline{B}/B_0}d\lambda\frac{\lambda\oint d\tau(\overline{B}/B_0)/\oint d\tau}{\omega_D\sqrt{1-\lambda B_0/\overline{B}}}+H_{res}\,,\\
F &= \frac{\left\langle B_0^{-2}\right\rangle^{-1}\omega_{*h}}{4\overline{B}^2}\int_0^{\overline{B}/B_0}\frac{\lambda d\lambda}{\omega_D\sqrt{1-\lambda B_0/\overline{B}}}+F_{res}\,,\\
I &= \frac{3\left\langle B_0^{-2}\right\rangle^{-2}\omega_{*h}(1+\eta_h)}{8\overline{B}^4}\int_0^{\overline{B}/B_0}d\lambda\frac{\lambda^2\oint d\tau(\overline{B}/B_0)/\oint d\tau}{\omega_D\sqrt{1-\lambda B_0/\overline{B}}}+I_{res}\,.
\end{aligned}
\tag{3.C2}
$$

To calculate the small imaginary corrections due to the weak resonance, we consider the speed integrals first and note from (3.C1) that they are all of the form of $\int_0^\infty \frac{f(t)e^{-t^2}dt}{\omega-At^2}=\int_0^\infty dt\frac{f(t)e^{-t^2}}{2A\sqrt{\omega/A}}\left(\frac{1}{\sqrt{\omega/A}-t}+\frac{1}{\sqrt{\omega/A}+t}\right)$, with f being only a function of t. The imaginary part of the preceding integral is given by $-\pi i\frac{e^{-\omega/A}f\left(\sqrt{\omega/A}\right)}{2A\sqrt{\omega/A}}$ from the calculus of residues. For the intermediate frequency ordering $\sqrt{\omega/A}<<1$, so that we can approximate the exponential by unity and only keep the largest contribution to $f\left(\sqrt{\omega/A}\right)$. As a result, for $\omega<<\langle\omega_{dh}\rangle\sim\omega_{*h}$, the weak hot electron drift resonance terms to lowest order can be written as

$$
\begin{aligned}
G_{res} &\approx -\frac{i\sqrt{\pi}\sqrt{\omega}\omega_{*h}\left(1-\frac{3}{2}\eta_h\right)B_0}{2\overline{B}}\int_0^{\overline{B}/B_0}\frac{d\lambda}{\omega_D^{3/2}\sqrt{1-\lambda B_0/\overline{B}}}\,,\\
H_{res} &\approx \frac{i\sqrt{\pi}\omega^{3/2}\omega_{*h}\left(1-\frac{3}{2}\eta_h\right)B_0}{2\overline{B}^3\left\langle B_0^{-2}\right\rangle}\int_0^{\overline{B}/B_0}d\lambda\frac{\lambda\oint d\tau(\overline{B}/B_0)/\oint d\tau}{\omega_D^{5/2}\sqrt{1-\lambda B_0/\overline{B}}}\,,\\
F_{res} &\approx \frac{i\sqrt{\pi}\omega^{3/2}\omega_{*h}\left(1-\frac{3}{2}\eta_h\right)}{2\overline{B}^2\left\langle B_0^{-2}\right\rangle}\int_0^{\overline{B}/B_0}\frac{\lambda d\lambda}{\omega_D^{5/2}\sqrt{1-\lambda B_0/\overline{B}}}\,,\\
I_{res} &\approx \frac{i\sqrt{\pi}\omega^{5/2}\omega_{*h}\left(1-\frac{3}{2}\eta_h\right)}{2\overline{B}^4\left\langle B_0^{-2}\right\rangle^2}\int_0^{\overline{B}/B_0}d\lambda\frac{\lambda^2\oint d\tau(\overline{B}/B_0)/\oint d\tau}{\omega_D^{7/2}\sqrt{1-\lambda B_0/\overline{B}}}\,.
\end{aligned}
\tag{3.C3}
$$

Once the above expressions are flux surface averaged, they reduce to the ones given in Eq. (3.41) upon using $\langle \omega_{dh} \rangle = \langle \omega_{de} \rangle T_h / T_e$.

References

[1] A. Hasegawa, Comments on Plasma Phys. Controlled Fusion **1**, 147 (1987).

[2] J. Kesner, L. Bromberg, M. E. Mauel and D. T. Garnier, *17th IAEA Fusion Energy Conference, Yokahama, Japan, 1998 (International Atomic Energy Agency, Vienna, 1999)*, Paper IAEA-F1-CN-69-ICP/09.

[3] I. B. Bernstein, E. A. Frieman, M. D. Kruskal and R. M. Kulsrud, *Proc. Roy. Soc.* London, Ser. A **244**, 17 (1958).

[4] D. Garnier, J. Kesner, M. Mauel, Phys. Plasmas **6**, 3431 (1999).

[5] A. N. Simakov, P.J. Catto, S.I. Krasheninnikov and J. J. Ramos, Phys. Plasmas **7**, 2526 (2000).

[6] J. Kesner, A. N. Simakov, D. T. Garnier, P.J. Catto, R. J. Hastie, S.I. Krasheninnikov, M. E. Mauel, T. Sunn Pedersen and J. J. Ramos, Nucl. Fusion **41**, 301 (2001).

[7] A. Hansen, D. Garnier, J. Kesner, M. Mauel and A. Ram, in *Proceedings of the 14th Topical Conference on Radio Frequency Power in Plasmas* (AIP Conf. Proceedings No. 595), edited by S. Bernanei and F. Paoletti (American Institute of Physics, New York, 2001) p. 362.

[8] D. B. Nelson, Phys. Fluids **23**, 1850 (1980).

[9] C.Z. Cheng, Fusion Tech. **18**, 443 (1990).

[10] M. J. Gerver and B. G. Lane, Phys. Fluids **29**, 2214 (1986).

[11] A. N. Simakov, R. J. Hastie and P.J. Catto, Phys. Plasmas **9**, 201 (2002).

[12] T. M. Antonsen and B. Lane, Phys. Fluids **23**, 1205 (1980).

[13] P.J. Catto, W. M. Tang and D. E. Baldwin, Plasma Physics **23**, 639 (1981).

[14] J.P. Freidberg, *Ideal Magnetohydrodynamics* (Plenum, New York, 1987).

[15] J. Kesner, N. Krasheninnikova and P.J. Catto, in *Poster Session of the 47th Annual Meeting of the Division of Plasma Physics, (APS)* (BP1.31) October 24-28 Denver, Colorado.

[16] N. Krasheninnikova and P.J. Catto, Phys. Plasmas, **12**, 32101 (2005).

[17] S. I. Krasheninnikov, P. J. Catto, and R. D. Hazeltine, Phys. Plasmas **7**, 1831 (2000).

[18] D. T. Garnier, et. al. *"Production and Study of High-Beta Plasma Confined by a Superconducting Dipole Magnet"* To be published in Phys. Plasmas in 2006.